

Bifidobacterium bifidum strains synergize with immune checkpoint inhibitors to reduce tumour burden in mice

Se-Hoon Lee^{1,2,15}, Sung-Yup Cho^{3,4,15}, Youngmin Yoon^{5,15}, Changho Park^{6,15}, Jinyoung Sohn⁶, Jin-Ju Jeong⁶, Bu-Nam Jeon⁶, Mongjoo Jang⁶, Choa An⁶, Suro Lee⁶, Yun Yeon Kim⁶, Gihyeon Kim⁵, Sujeong Kim⁵, Yunjae Kim⁵, Gwang Bin Lee⁷, Eun Ju Lee⁶, Sang Gyun Kim⁶, Hong Sook Kim¹, Yeongmin Kim⁵, Hyun Kim⁵, Hyun-Suk Yang⁸, Sarang Kim⁸, Seonggon Kim⁹, Hayung Chung¹⁰, Myeong Hee Moon⁷, Myung Hee Nam¹⁰, Jee Young Kwon¹¹, Sungho Won¹², Joon-Suk Park^{9,16}, George M. Weinstock^{11,16}, Charles Lee^{11,13,14,16}, Kyoung Wan Yoon^{6,8} ✉ and Hansoo Park^{5,6} ✉

The gut microbiome can influence the development of tumours and the efficacy of cancer therapeutics^{1–5}; however, the multi-omics characteristics of antitumour bacterial strains have not been fully elucidated. In this study, we integrated metagenomics, genomics and transcriptomics of bacteria, and analyses of mouse intestinal transcriptome and serum metabolome data to reveal an additional mechanism by which bacteria determine the efficacy of cancer therapeutics. In gut microbiome analyses of 96 samples from patients with non-small-cell lung cancer, *Bifidobacterium bifidum* was abundant in patients responsive to therapy. However, when we treated syngeneic mouse tumours with commercial strains of *B. bifidum* to establish relevance for potential therapeutic uses, only specific *B. bifidum* strains reduced tumour burden synergistically with PD-1 blockade or oxaliplatin treatment by eliciting an antitumour host immune response. In mice, these strains induced tuning of the immunological background by potentiating the production of interferon- γ , probably through the enhanced biosynthesis of immune-stimulating molecules and metabolites.

Recent reports have distinguished the gut microbiome as an important regulator of innate and adaptive immunity^{6–8}, with the potential to modulate responses to chemotherapeutic agents such as cyclophosphamide and oxaliplatin^{1–3}, as well as immunotherapeutic agents such as anti-CTLA-4 and anti-PD-1 antibodies^{4,5,9–11}. However, the specific functions and molecular mechanisms of each component of the complex gut microbiome remain largely unknown. In this study, we sought to identify the strain-specific effect of the microbiome that influences cancer development and the efficacy of cancer therapeutics in patients diagnosed with non-small-cell lung cancer (NSCLC). Furthermore, we

investigated the molecular mechanisms underlying the effects of specific strains through multi-omics analyses using patient samples, syngeneic mouse tumour models and isolated microbes (Extended Data Fig. 1a).

To examine whether specific microbial signatures could be observed in patients with NSCLC, we performed 16S ribosomal RNA (rRNA) sequencing on stool samples collected from 96 patients with NSCLC and 139 healthy controls (Fig. 1a). Detailed clinical information for each group is provided in Supplementary Tables 1 and 2. Based on these data, we compared the diversity of gut microbiomes and found that α -diversity (Shannon index) and β -diversity (unweighted UniFrac) significantly differed between the two groups (Extended Data Fig. 1b,c). Using linear discriminant analysis of effect size (LEfSe), we observed that *Prevotella copri* and *Faecalibacterium prausnitzii* were enriched in healthy controls, whereas *Enterococcus* and *Lactobacillus* were enriched in patients with NSCLC (Extended Data Fig. 1d). Next, we determined whether responsiveness to cancer therapeutics such as platinum-based chemotherapy ($n=58$), immune checkpoint blockade ($n=22$) or epidermal growth factor receptor tyrosine kinase inhibitor (EGFR TKI; $n=16$) was associated with the gut microbiome of patients with NSCLC. Patients with a partial response (PR) were classified as responders ($n=54$), whereas those with stable disease (SD) or progressive disease (PD) were classified as non-responders ($n=42$) according to the response evaluation criteria in solid tumours (RECIST), v.1.1 (ref. ¹²) (Fig. 1a). There were no significant differences observed in body mass index (BMI), smoking, alcohol and serum glucose levels between responders and non-responders (Supplementary Table 3). We detected significant differences in α -diversity and β -diversity between the two groups. (Fig. 1b,c).

¹Division of Hematology–Oncology, Department of Internal Medicine, Samsung Medical Center, Sungkyunkwan University School of Medicine, Seoul, Korea. ²Department of Health Sciences and Technology, SAIHST, Sungkyunkwan University School of Medicine, Seoul, Korea. ³Department of Biomedical Sciences, Seoul National University College of Medicine, Seoul, Korea. ⁴Cancer Research Institute, Seoul National University College of Medicine, Seoul, Korea. ⁵Department of Biomedical Science and Engineering, Gwangju Institute of Science and Technology (GIST), Gwangju, Korea. ⁶Genome and Company, Gyeonggi-do, Korea. ⁷Department of Chemistry, Yonsei University, Seoul, Korea. ⁸Department of Biotechnology, Hoseo University, Asan, Korea. ⁹Laboratory Animal Center, Daegu-Gyeongbuk Medical Innovation Foundation (DGMIF), Daegu, Korea. ¹⁰Korea Basic Science Institute, Seoul Center, Seoul, Korea. ¹¹The Jackson Laboratory for Genomic Medicine, Farmington, CT, USA. ¹²Department of Public Health Sciences, Seoul National University, Seoul, Korea. ¹³Department of Life Science, Ewha Womans University, Seoul, Korea. ¹⁴The First Affiliated Hospital of Xi'an Jiaotong University, Xi'an, China. ¹⁵These authors contributed equally: Se-Hoon Lee, Sung-Yup Cho, Youngmin Yoon and Changho Park. ¹⁶These authors jointly supervised this work: Joon-Suk Park, George M. Weinstock and Charles Lee. ✉e-mail: kwyoong8@gmail.com; hspark27@gist.ac.kr

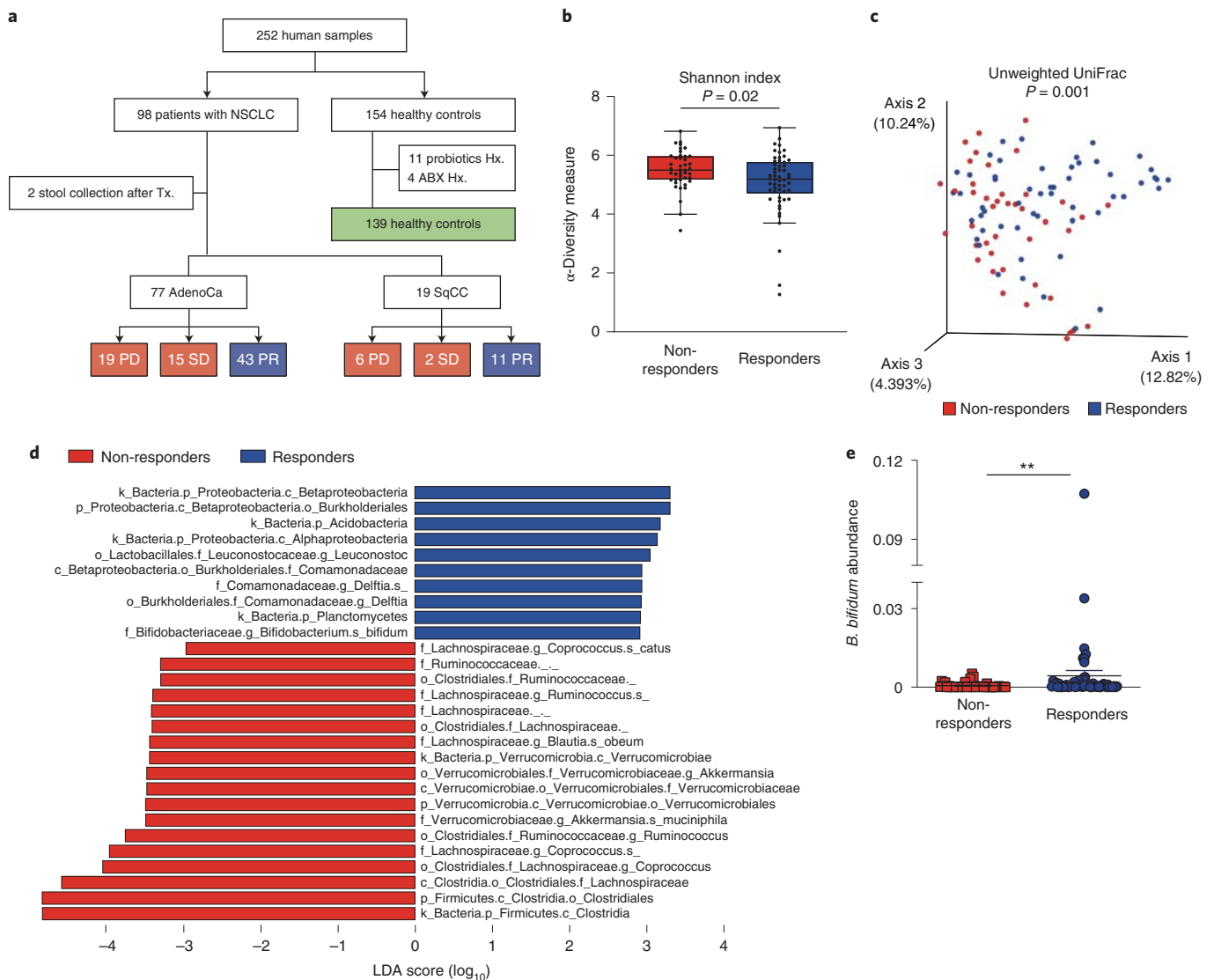


Fig. 1 | Marker gene sequence (16S rRNA) profiling of the gut microbiome in patients with NSCLC. a, Patient enrolment, treatment and response details. A total of 252 human samples (98 patients with NSCLC and 154 healthy controls) were enrolled. However, 2 patients with NSCLC (stool collection after treatment) and 15 healthy controls (probiotics history, $n = 11$ and antibiotics history, $n = 4$) were excluded from analysis. Finally, a total of 235 human samples (96 patients with NSCLC and 139 healthy controls) were analysed. The 96 patients with NSCLC (stage IIIB and IV) were divided into responders (PR, $n = 54$) and non-responders (SD + PD, $n = 42$) according to the RECIST 1.1 criteria: AdenoCa, adenocarcinoma; Hx., history; SqCC, squamous cell carcinoma; Tx., treatment. **b, c**, Box-and-whisker plot illustrating the α -diversity (**b**) and principal coordinate analysis plot illustrating the β -diversity (**c**) of gut microbiomes in non-responders ($n = 42$) and responders ($n = 54$) in patients with NSCLC. P value of α -diversity calculated using Kruskal–Wallis test. Boxes represent the first and third quartiles and the median, and whiskers represent ranges up to 1.5 \times the interquartile ranges. **d**, A plot of LDA scores from the LefSe method illustrating the differential abundance of the indicated taxa in the gut microbiomes of non-responders and responders (LDA score > 2.8). **e**, The abundance of *B. bifidum* in patients with NSCLC ($n = 96$) was determined by qPCR. Data show the mean \pm s.e.m. The P value was calculated using two-sided unpaired Mann–Whitney U -test, $**P = 0.0022$.

The LefSe analysis revealed that *B. bifidum*, specified to the species level, was significantly enriched in responders, whereas *Akkermansia muciniphila* and *Blautia obeum* were enriched in non-responders (Fig. 1d and Supplementary Table 4). Oral administration of *Bifidobacterium* spp. is reported to enhance the therapeutic efficacy of PD-1 blockade by facilitating dendritic cell maturation⁴. To confirm that *B. bifidum* was more abundant in responders, we conducted quantitative PCR (qPCR) using DNA extracted from stool samples. We found significantly increased abundance of *B. bifidum* in responders compared with non-responders (Fig. 1e). Most patients (15 out of 16) treated with EGFR TKI were classified

as responders, and *B. bifidum* was markedly enriched in the responders compared with non-responders, even when the patients treated with EGFR TKI were excluded (Extended Data Fig. 1e). In addition, we compared interferon- γ (IFN- γ) production elicited by *B. bifidum* or *Leuconostoc* strains, which were enriched in responders according to the LefSe analysis, using an in vitro co-culture system. *B. bifidum* strains elicited significantly more IFN- γ secretion than *Leuconostoc* strains (Extended Data Fig. 1f). Conclusively, metagenomic, qPCR and in vitro analyses demonstrated an increased abundance of *B. bifidum* in responders compared with non-responders.

To determine whether *B. bifidum* modulates the response to cancer therapeutics, we supplemented murine models of syngeneic tumours with each of the following four *B. bifidum* strains (Fig. 2a and Supplementary Table 5): *B. bifidum* KCTC3357 (*B. bif_K57*), *B. bifidum* KCTC3418 (*B. bif_K18*), *B. bifidum* Bb-06 (*B. bif_B06*) and *B. bifidum* Rosell-71 (*B. bif_R71*). Commercial *B. bifidum* strains were used because bacterial isolation from patients is technically challenging. First, we evaluated the presence and colonization of *B. bifidum* strains in the gut. Following oral administration, *B. bifidum* was increased in faecal samples after 4 h, but its abundance was significantly reduced after 24 h, which indicates that *B. bifidum* is not colonizing but transiently localized in the mouse intestine (Extended Data Fig. 2a). This suggests that daily administration of *B. bifidum* is required to evaluate its antitumour effects. Although all four *B. bifidum* strains decreased tumour growth relative to control mice, only two *B. bifidum* strains (*B. bif_K57* and *B. bif_K18*) worked synergistically with oxaliplatin to reduce tumour growth (Fig. 2b). To further investigate the synergistic effect of specific *B. bifidum* strains with oxaliplatin, we performed immunological analyses of mice treated with synergistic *B. bif_K57* and non-synergistic *B. bif_B06*. Immune cell profiling revealed that the two *B. bifidum* strains decreased the regulatory T (T_{reg}) cell population while increasing the population of $CD4^+$ T, $CD8^+$ T, effector $CD8^+$ T and natural killer (NK) cells in the spleen and tumours (Supplementary Fig. 1). Relative to oxaliplatin treatment, treatment with oxaliplatin plus *B. bif_K57* significantly increased the population of antitumour lymphocytes, including $CD8^+$ T and effector $CD8^+$ T cells, and augmented the $CD8^+$ T/ T_{reg} cell and effector $CD8^+$ T/ T_{reg} cell ratios in the spleen and tumours. However, the oxaliplatin plus *B. bif_B06* treatment did not elicit these effects (Extended Data Fig. 2b and Supplementary Fig. 1). Expression profiling of intratumoural cytokines revealed significant increases in IFN- γ and interleukin-2 (IL-2) and significant decreases in tumour necrosis factor- α (TNF- α) and IL-10 in mice treated with oxaliplatin plus *B. bif_K57* relative to those treated with oxaliplatin alone (Extended Data Fig. 2c). These effects were weaker in mice treated with oxaliplatin plus *B. bif_B06* (Extended Data Fig. 2c).

Next, we used the syngeneic tumour model to investigate the possibility that *B. bifidum* strains control the response of the immune checkpoint blockade (Fig. 2a). Similar to our observations

in oxaliplatin-treated groups, only specific *B. bifidum* strains (*B. bif_K57*, *B. bif_K18* and *B. bifidum* MG731 (*B. bif_M31*)) worked synergistically with anti-PD-1 to decrease tumour growth, whereas other *B. bifidum* strains (*B. bif_B06*, *B. bif_R71* and *B. bifidum* CKDB001 (*B. bif_C01*)) showed no synergistic effects with anti-PD-1 (Fig. 2c and Extended Data Fig. 2d,e). The differences in therapeutic efficacy were accompanied by the expression of intratumoural cytokines and differences in profiles of spleen and tumour immunocytes. The spleen and tumour population of antitumour lymphocytes ($CD4^+$ T, $CD8^+$ T and NK cells) and the $CD8^+$ T/ T_{reg} cell and effector $CD8^+$ T/ T_{reg} cell ratios increased in mice treated with synergistic *B. bifidum* strains plus anti-PD-1 relative to those in mice treated with anti-PD-1 alone (Fig. 2d and Supplementary Figs. 2 and 3). Moreover, *B. bif_K57* significantly increased the expression of IFN- γ and IL-2 and decreased the expression of TNF- α and IL-10 in tumours (Fig. 2e). Moreover, mice treated with anti-PD-1 plus *B. bif_K57* exhibited increased levels of cytokine-producing IL-2 $^+$ CD4 $^+$ and IFN- γ^+ CD8 $^+$ tumour-infiltrating T cells compared with mice treated with anti-PD-1 alone or anti-PD-1 plus *B. bif_B06* (Fig. 2f). These results show that increased levels of IL-2 and IFN- γ in mice treated with anti-PD-1 plus a synergistic *B. bifidum* strain are associated with activated T cells in tumours. To evaluate the correlation of *B. bifidum*-mediated immune regulation between the primary site (intestine) and the target site (tumour), we performed mice intestine immune cell profiling. Consistent with the spleen and tumour results, mice treated with anti-PD-1 plus *B. bif_K57* showed a significantly increased population of $CD4^+$ T, $CD8^+$ T, effector $CD8^+$ T and NK cells in the intestine compared with mice treated with anti-PD-1 alone (Fig. 2g and Extended Data Fig. 2f).

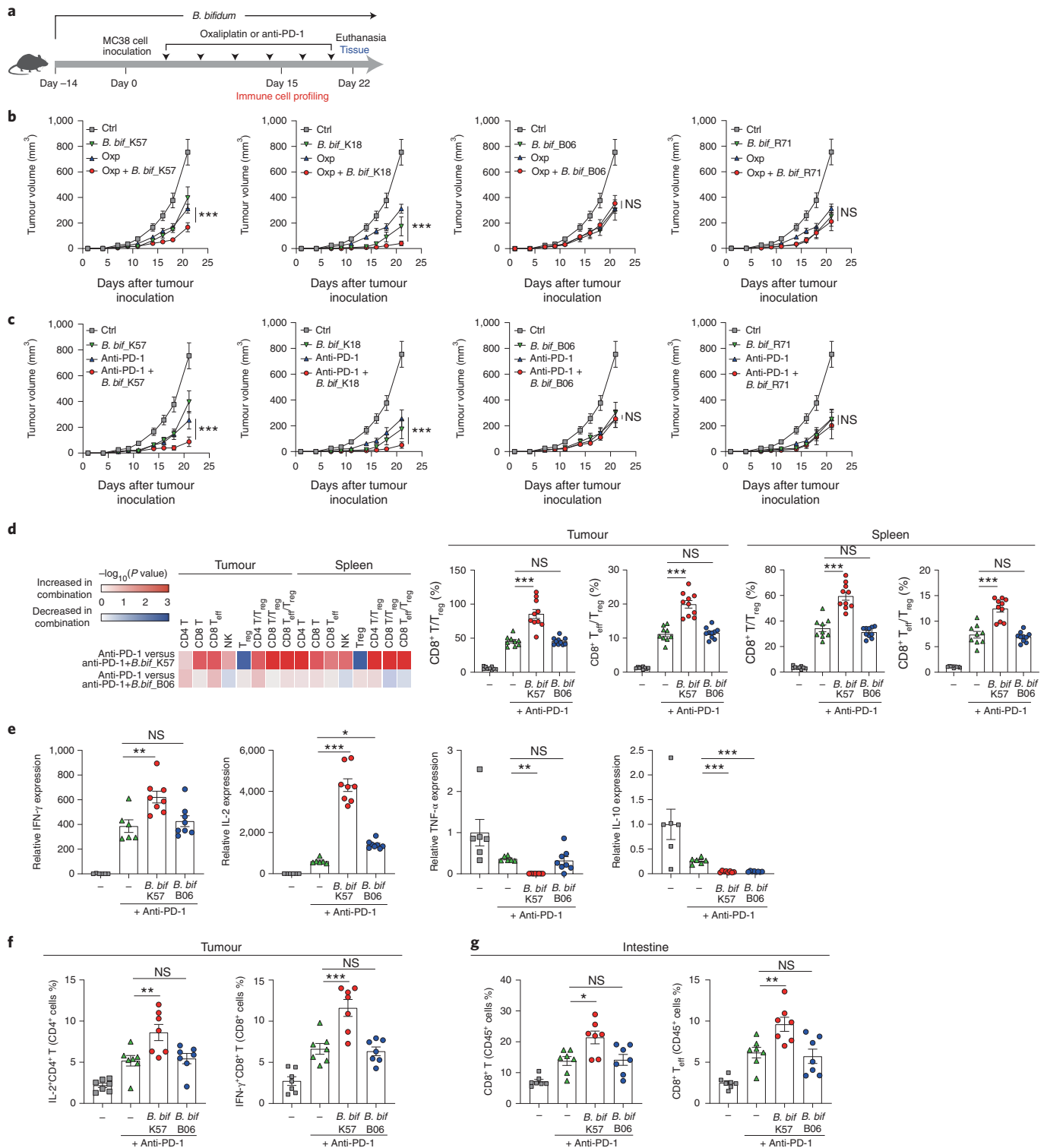
To elucidate the molecular mechanisms by which specific *B. bifidum* strains work synergistically with anticancer therapeutics, we performed RNA sequencing of intestinal tissues collected from syngeneic tumour mice treated with anti-PD-1 plus synergistic (*B. bif_K57*) or non-synergistic *B. bifidum* strains (*B. bif_B06*). We observed a significant increase in genes associated with Gene Ontology (GO) terms “lymphocyte activation”, “interferon-gamma production” and “positive regulation of interferon-gamma production” in mice treated with anti-PD-1 plus *B. bif_K57* compared with those treated with anti-PD-1 plus *B. bif_B06* (Fig. 3a, Extended Data Fig. 3a and Supplementary Table 6). Serum metabolic

Fig. 2 | Synergistic antitumour effect of *B. bifidum* strains in combination with oxaliplatin or anti-PD-1 in syngeneic mouse tumour models. **a**, Schematic of the experimental timeline: 14 days after initial oral administration of *B. bifidum* strains, mice were inoculated with MC38 colon cancer cells, and oxaliplatin (Oxp) or anti-PD-1 was intraperitoneally injected. **b**, Tumour growth curves showing the changes in tumour volumes after administration of *B. bifidum*, with or without oxaliplatin. The number of mice per group was as follows: control (Ctrl), $n=7$; Oxp or *B. bif_K57* or *B. bif_B06* or Oxp + *B. bif_K57* or Oxp + *B. bif_B06*, $n=8$; *B. bif_K18* or Oxp + *B. bif_K18*, $n=7$; *B. bif_R71* or Oxp + *B. bif_R71*, $n=6$. P values: Oxp versus Oxp + *B. bif_K57*, $P=0.0004$; Oxp versus Oxp + *B. bif_K18*, $P=0.0001$. **c**, Tumour growth curves showing the changes in tumour volume after administration of *B. bifidum* strains, with or without anti-PD-1. The number of mice per group was as follows: Control or anti-PD-1, $n=7$; *B. bif_K57* or *B. bif_B06* or anti-PD-1 + *B. bif_K57* or anti-PD-1 + *B. bif_B06*, $n=8$; *B. bif_K18* or anti-PD-1 + *B. bif_K18*, $n=7$; *B. bif_R71*, $n=7$; anti-PD-1 + *B. bif_R71*, $n=6$. P values: anti-PD-1 versus anti-PD-1 + *B. bif_K57*, $P<0.0001$; anti-PD-1 versus anti-PD-1 + *B. bif_K18*, $P<0.0001$. **d**, Flow cytometry analyses were performed on mouse spleen and tumour tissue. Left: the heatmap represents the P values of differences in the immune cell profile between anti-PD-1 treatment and combined treatment of anti-PD-1 and *B. bifidum* strains. Exact P values are provided in Supplementary Table 14. Right: ratios of $CD8^+$ T/ T_{reg} and effector $CD8^+$ T (T_{eff})/ T_{reg} cells in the spleens and tumours. The number of mice per group was as follows: control or anti-PD-1, $n=9$; anti-PD-1 + *B. bif_K57* or *B. bif_B06*, $n=10$. P values: anti-PD-1 versus anti-PD-1 + *B. bif_K57*, $P<0.0001$ (ratio of $CD8^+$ T/ T_{reg} and effector $CD8^+$ T/ T_{reg} , tumour); anti-PD-1 versus anti-PD-1 + *B. bif_K57*, $P<0.0001$ (ratio of $CD8^+$ T/ T_{reg} and effector $CD8^+$ T/ T_{reg} , spleen). **e**, Cytokine expression profiles in tumours from mice treated with anti-PD-1 or both anti-PD-1 and *B. bifidum*, as measured by qPCR. Control and anti-PD-1 groups, $n=6$ independent biological replicates per group; anti-PD-1 + *B. bif_K57* or *B. bif_B06* groups, $n=8$ independent biological replicates per group. P values were calculated using one-way ANOVA with Tukey's test for multiple comparison within anti-PD-1 treated groups. IFN- γ of anti-PD-1 versus anti-PD-1 + *B. bif_K57*, $P=0.0084$; IL-2 of anti-PD-1 versus anti-PD-1 + *B. bif_K57*, $P<0.0001$; IL-2 of anti-PD-1 versus anti-PD-1 + *B. bif_B06*, $P=0.0351$; TNF- α of anti-PD-1 versus anti-PD-1 + *B. bif_K57*, $P=0.002$; IL-10 of anti-PD-1 versus anti-PD-1 + *B. bif_K57*, $P<0.0001$; IL-10 of anti-PD-1 versus anti-PD-1 + *B. bif_B06*, $P<0.0001$. **f**, Flow cytometry analysis of IL-2 $^+$ CD4 $^+$ and IFN- γ^+ CD8 $^+$ T cells in tumours. $n=7$ mice per group. P values: IL-2 $^+$ CD4 $^+$ T cells of anti-PD-1 versus anti-PD-1 + *B. bif_K57*, $P=0.0075$; IFN- γ^+ CD8 $^+$ T cells of anti-PD-1 versus anti-PD-1 + *B. bif_K57*, $P=0.0003$. **g**, Flow cytometry analysis of $CD8^+$ and effector $CD8^+$ T cells in the lamina propria of the intestine. $n=7$ mice per group. P values: $CD8^+$ T cells of anti-PD-1 versus anti-PD-1 + *B. bif_K57*, $P=0.0107$; effector $CD8^+$ T cells of anti-PD-1 versus anti-PD-1 + *B. bif_K57*, $P=0.0099$. For all graphs, data are shown as the mean \pm s.e.m.; * $P<0.05$, ** $P<0.01$, *** $P<0.001$; NS, not significant. P values were calculated using two-way (**b**, **c**) or one-way (**d** (right), **e**–**g**) ANOVA with Tukey's test for multiple comparison, or two-sided unpaired t -test (**d**, left).

profiling revealed that several molecules, including L-tryptophan, uric acid and *N*-acetyl zonisamide, were increased in mice treated with anti-PD-1 plus *B. bif*_K57 relative to mice treated with anti-PD-1 plus *B. bif*_B06 (Fig. 3b). In vitro, L-tryptophan treatment increased IFN- γ production from activated CD8⁺ T cells (Fig. 3c). In the principal component analysis of lipidomic profiling data, mice treated with anti-PD-1, anti-PD-1 plus *B. bif*_B06 or anti-PD-1 plus *B. bif*_K57 clustered as separate groups (Extended Data Fig. 3b). Overall serum lipid levels were lower in *Bifidobacterium*-treated mice than

in mice treated with anti-PD-1 alone. Furthermore, the magnitude of lipid serum decrease was enhanced when *Bifidobacterium* was combined with anti-PD-1, especially in the anti-PD-1 plus *B. bif*_K57 group (Extended Data Fig. 3c). A previous study¹³ showed that lipid challenge decreases IFN- γ secretion by T cells.

The intestine transcriptomic, serum metabolomic and lipidomic data suggested that the synergistic effect of *B. bif*_K57 was strongly associated with IFN- γ , which plays a critical role in tumour immunity^{14,15}. When we injected an IFN- γ receptor (IFN γ R)-blocking



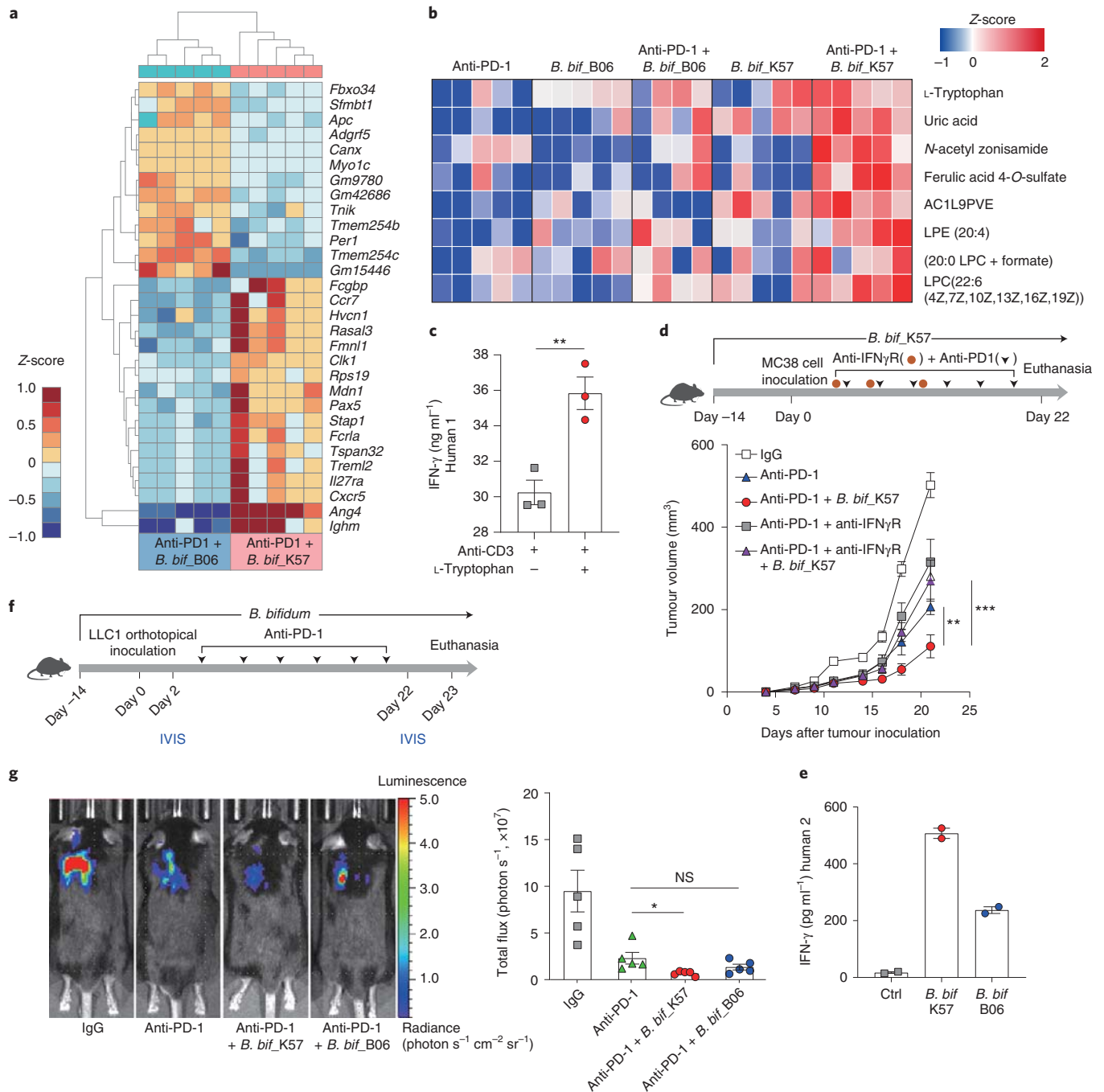


Fig. 3 | Transcriptomics and metabolomics analysis of syngeneic tumour models treated with *B. bifidum* strains. **a**, Heatmap showing differentially expressed genes between mice treated with anti-PD-1 + *B. bif_K57* and anti-PD-1 + *B. bif_B06*, as determined by RNA sequencing of intestinal tissues. Columns represent mice and rows represent genes (FDR < 0.05). **b**, Heatmap depicting differentially detected metabolites from the serum of syngeneic mice; AC1L9PVE, 2',3'-dideoxy-N-((4-methoxyphenyl)diphenylmethyl)-5'-O-((4-methoxyphenyl)diphenylmethyl)-2'-(1-piperidinyl)-adenosine. **c**, Human CD8⁺ T cells were stimulated with plate-bound anti-CD3 antibody or a combination of anti-CD3 antibody and L-tryptophan. The levels of IFN- γ in supernatant were measured by ELISA. Three technical replicates were performed. The *P* value was calculated using two-sided unpaired *t*-test; *P* = 0.0082. **d**, Upper: schematic of experimental timeline: 14 days after initial oral administration of *B. bif_K57*, mice were inoculated with MC38 colon cancer cells, and anti-PD-1 (twice a week) or anti-IFN γ R (50 μ g, days 1, 6 and 11) was administered via intraperitoneal injection. Lower: MC38 tumour growth curves are shown for animals subjected to the indicated experimental treatments. *n* = 5 mice per group. *P* values were calculated using two-way ANOVA with Tukey's test for multiple comparison. Anti-PD-1 + *B. bif_K57* versus anti-PD-1 + anti-IFN γ R + *B. bif_K57*, *P* < 0.0001; anti-PD-1 versus anti-PD-1 + *B. bif_K57*, *P* = 0.0013. **e**, Effect of *B. bifidum* strains on the in vitro stimulation of CD8⁺ T cells by monocytes. Secreted IFN- γ was measured by ELISA in co-cultures of human autologous T cells and monocytes treated with *B. bif_K57* or *B. bif_B06*. Two technical replicates were performed. **f**, Schematic of experimental timeline: 14 days after initial oral administration of *B. bifidum*, mice were orthotopically inoculated with LLC1 cells, and anti-PD-1 was administered via intraperitoneal injection (twice a week). Bioluminescence images were acquired using an in vivo imaging systems (IVIS) Spectrum CT. **g**, Left: representation of bioluminescence images. The colour scale depicts photon flux. Right: total flux measurements (*n* = 5 per group) at day 22. *P* values were calculated using Welch's ANOVA with Tukey's test for multiple comparison within anti-PD-1 treated groups. Anti-PD-1 versus anti-PD-1 + *B. bif_K57*, *P* = 0.038. For all graphs, data show the mean \pm s.e.m.; **P* < 0.05, ***P* < 0.01, ****P* < 0.001.

antibody into syngeneic mice, we found that IFN γ R blockade abrogated the tumour-reducing effects of both anti-PD-1 and anti-PD-1 plus *B. bif_K57* (Fig. 3d). Next, we compared *B. bifidum*-induced IFN- γ production between synergistic *B. bif_K57* and non-synergistic *B. bif_B06* using an in vitro system. We found that *B. bif_K57* elicited significantly more IFN- γ secretion than *B. bif_B06* (Fig. 3e and Extended Data Fig. 4a). To determine whether *B. bifidum* is sufficient to enhance anti-PD-1 efficacy without the effects of other commensal microbiota, we treated mice with an antibiotic cocktail (ABX) supplemented in drinking water before administration of *B. bif_K57* (Extended Data Fig. 4b). Mice were administered ABX or water, and stool samples were collected on days 0 and 14. The abundance of bacterial 16S rRNA gene sequences was significantly reduced in ABX-treated mice compared with water-treated mice (Extended Data Fig. 4c), which indicates a significant decrease in intestinal bacteria. Although the efficacy of anti-PD-1 was lower in ABX-treated mice than in PBS-treated mice, mice treated with anti-PD-1 plus *B. bif_K57* after ABX administration exhibited significantly reduced tumour growth relative to PBS-treated or ABX-treated mice, which received only anti-PD-1 (Extended Data Fig. 4b).

Next, we validated the synergistic effect of anti-PD-1 and *B. bif_K57* in lung cancer models. We performed experiments using subcutaneous and orthotopic lung cancer models with Lewis lung carcinoma (LLC1) cells (Fig. 3f and Extended Data Fig. 4d). As shown through bioluminescence monitoring, *B. bif_K57* worked synergistically with anti-PD-1 to reduce tumour growth (Fig. 3g). Furthermore, an increased reduction in tumour size was observed in mice treated with anti-PD-1 plus *B. bif_K57* compared with mice treated with anti-PD-1 alone or anti-PD-1 plus *B. bif_B06* (Extended Data Fig. 4d,e). In addition, *B. bif_K57* administration increased the antitumour effect of anti-PD-1 even in syngeneic models with anti-PD-1-resistant 4T1 breast cancer cells (Extended Data Fig. 4f). Although when used separately, anti-PD-1 and *B. bif_K57* showed little antitumour effects, mice treated with anti-PD-1 plus *B. bif_K57* showed significantly decreased 4T1 tumour cell growth (Extended Data Fig. 4f). These data suggest that the synergistic effect of this *B. bifidum* strain with anti-PD-1 treatment may be applicable to anti-PD-1-resistant cancers.

To determine the genetic bases underlying the different antitumour immune responses observed in mice inoculated with synergistic and non-synergistic *B. bifidum* strains, we performed whole-genome sequencing (WGS) and whole-transcriptome sequencing (WTS) of these bacteria. The average genome length was 2,212,688 bp, with 1,807 predicted genes and 62.7% GC content (Supplementary Table 7). Average nucleotide identity (ANI) analysis revealed that non-synergistic *B. bifidum* strains (*B. bif_B06*, *B. bif_R71* and *B. bif_C01*) were more similar to each other than to the synergistic *B. bifidum* strains (*B. bif_K57* and *B. bif_K18*) (Fig. 4a). The synergistic strains were predicted to encode 501 genes that were not present in the genomes of non-synergistic strains, whereas 232 genes that were commonly encoded by the non-synergistic strains were not detected in the genomes of synergistic strains (Fig. 4b). Transcriptome analyses identified a total of 45 annotated genes that were significantly upregulated in the synergistic *B. bifidum* strains, and a total of 23 annotated genes that were significantly upregulated in the non-synergistic *B. bifidum* strains (false discovery rate (FDR) < 0.1; Supplementary Tables 8 and 9). GO enrichment analysis revealed that terms related to “peptidoglycan biosynthetic process” and “cell wall biogenesis” were significantly enriched in synergistic *B. bifidum* strains (FDR < 0.1; Fig. 4c and Supplementary Table 10). Next, we estimated the peptidoglycan levels of *B. bifidum* strains and found that the amount of peptidoglycan was significantly increased in *B. bif_K57* compared with *B. bif_B06* (Extended Data Fig. 5). Genes associated with the peptidoglycan biosynthetic process, such as *MurE* and *GlmM*, were highly expressed

in the stools of mice treated with anti-PD-1 plus *B. bif_K57* compared with anti-PD-1 plus *B. bif_B06* (Fig. 4d). The involvement of peptidoglycans in anticancer immune modulation was also supported by our analyses of stool samples from patients with NSCLC. We performed WGS on both *B. bifidum*-containing ($n = 14$) and *B. bifidum*-free ($n = 11$) stool samples. Functional profiling data (the HMP unified metabolic analysis network 2 (HUMAN2) result) using stool WGS revealed that the peptidoglycan biosynthesis pathway was enriched in responders containing *B. bifidum* (Fig. 4e and Supplementary Table 11). We also found that IFN- γ secretion of human T cells co-cultured with autologous monocytes preincubated with synergistic *B. bifidum* strains (*B. bif_K57* and *B. bif_K18*) were significantly inhibited by a Toll-like receptor 2 (TLR2)-blocking antibody (Fig. 4f). When we used *Tlr2* knockout (KO) mice for syngeneic tumour models, *B. bif_K57* had little synergistic effect with anti-PD-1 in *Tlr2* KO mice (Fig. 4g), which was in contrast to the results in wild-type mice (Fig. 2c). Given that TLR2 is critical for peptidoglycan recognition and stimulation of downstream immune responses¹⁶, these data suggest that activation of peptidoglycan-mediated IFN- γ signalling is a determining factor for the strain-specific synergistic effect of *Bifidobacterium* on cancer therapeutics.

Previous reports have shown that *Bifidobacterium* spp. is significantly more abundant in patients with metastatic melanoma who responded to PD-1 blockade¹¹, and elicits antitumour immunity^{4,11,17,18}, whereas another study showed *Ruminococcaceae* and *Faecalibacterium* are significantly enriched in responders with metastatic melanoma⁵. Moreover, *A. muciniphila* is linked to a favourable outcome to PD-1 blockade in epithelial tumours¹⁰. These results suggest that the immune-modulating effects of the gut microbiota are different according to race, geography and cancer types.

Through multi-omics approaches, we demonstrated that the *B. bifidum* strain-specific enhancement of anticancer immunity is due to IFN- γ signalling. We found that increased peptidoglycan biosynthesis in synergistic strains enhanced *B. bifidum*-induced IFN- γ production. We also showed that increased serum L-tryptophan is associated with *B. bifidum*-induced IFN- γ production. The composition of the gut microbiota is linked to the serum levels of L-tryptophan, an essential amino acid, since several types of commensal bacteria possess the tryptophan-degrading enzymes¹⁹. In addition, administration of *Bifidobacterium infantis* increased the plasma concentration of tryptophan in rats by inhibiting the tryptophan-metabolizing enzyme IDO²⁰. In this study, we found that anti-PD-1 plus *B. bif_K57* inhibited tumour growth and increased serum L-tryptophan levels, which suggests that *B. bif_K57* could modulate L-tryptophan-degrading enzymes.

Several studies have reported the lipid-lowering effects of *Bifidobacterium* spp. in human and animal models^{21–23}. The lipid levels affect T cells and cancer cells. Lipid challenge inhibits T-cell response through autophagy inhibition¹³, and lipid metabolism is associated with the differentiation and survival of several T cell subsets²⁴. Cancer cells exhibit high energy demands for proliferation, and lipids are the main source of energy generation in these cells. Plasma levels of several lipids increase in patients with cancer, and several lipid-lowering drugs are suggested to have antitumour effects²⁵. Therefore, lipid lowering can be one of the mechanisms through which *B. bifidum* achieves its antitumour effects.

The expression of intratumoral TNF- α was decreased in mice treated with a synergistic *B. bifidum* strain (Fig. 2e and Extended Data Fig. 2c). TNF- α is secreted by stromal cells, cancer cells and macrophages in the tumour microenvironment²⁶. Several studies have demonstrated that TNF- α exerts its immunosuppressive roles in cancers by recruiting several negative regulators of cancer immunity, including T_{reg}, B_{reg} and myeloid-derived suppressor cells^{27–29}. Furthermore, TNF- α inhibits tumour infiltration and enhances the

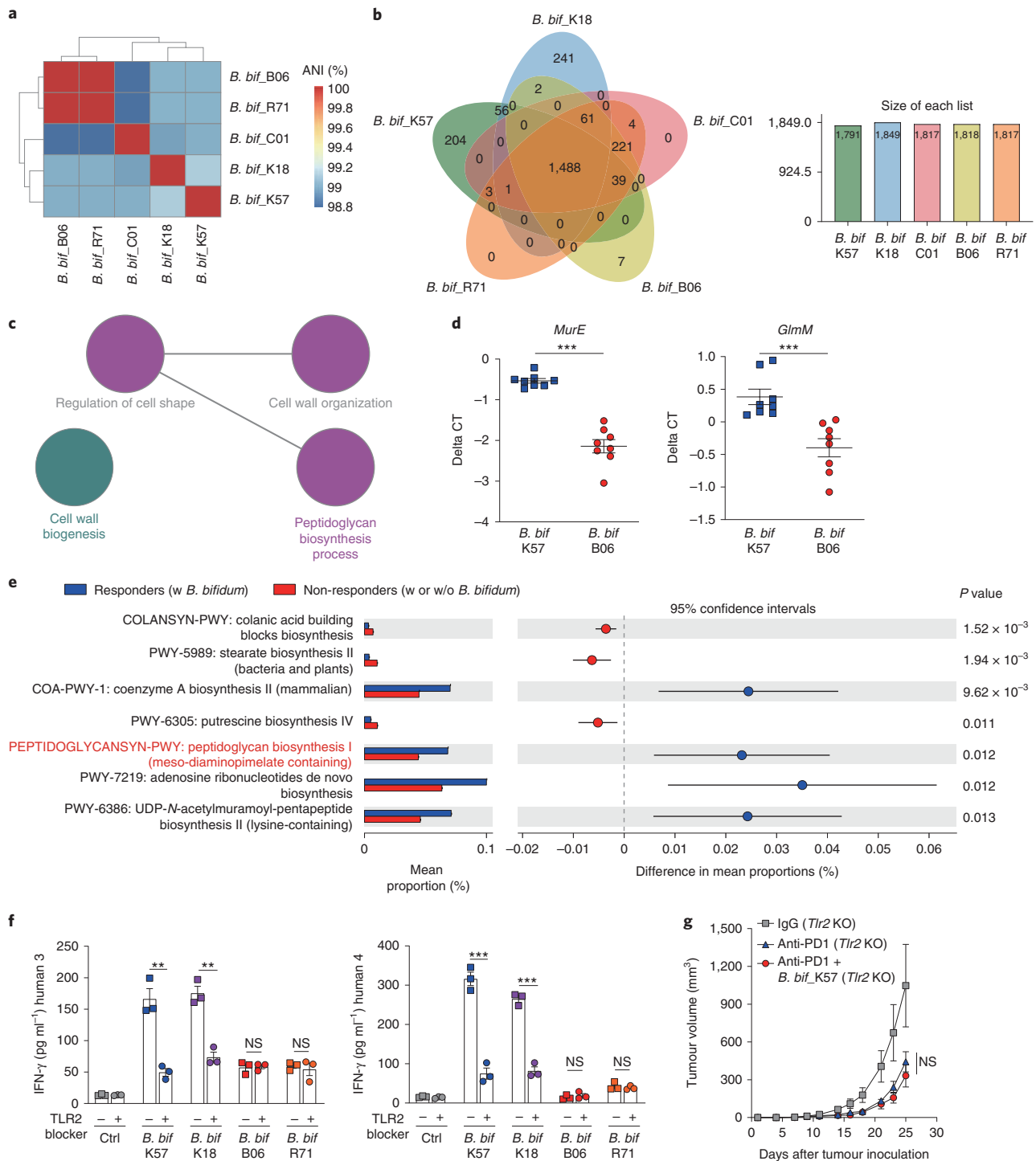


Fig. 4 | Comparative genomics and transcriptomics analyses of *B. bifidum* strains. **a**, Cluster plot illustrating the ANI of the five sequenced *B. bifidum* strains: *B. bif*_K57, *B. bif*_K18, *B. bif*_B06, *B. bif*_R71 and *B. bif*_C01. **b**, Left: Venn diagram illustrating the number of shared genes among the five *B. bifidum* strains. Right: Graph quantifying the total number of genes for each strain. **c**, Network graph representation of enriched GO biological processes (analysed by ClueGO, FDR < 0.1), enriched in synergistic *B. bifidum* strains (*B. bif*_K57 and *B. bif*_K18). **d**, Expression of genes associated with peptidoglycan biosynthesis process in the stool of mice treated with anti-PD-1 + *B. bifidum* strains (*B. bif*_K57 or *B. bif*_B06). *RecA* was used for normalization. *P* values were calculated using two-sided unpaired *t*-test. *MurE* of *B. bif*_K57 versus *B. bif*_B06, *P* < 0.0001; *GlmM* of *B. bif*_K57 versus *B. bif*_B06, *P* = 0.0008. **e**, Comparison of functional metagenome profiling was performed using HUMAnN2 between responders (PR = 12) with *B. bifidum* and non-responders (SD = 1, PD = 12) with or without (w or w/o) *B. bifidum*. *P* values were calculated using two-sided Welch's *t*-test. **f**, Effect of *B. bifidum* strains on the in vitro stimulation of CD8⁺ T cells by monocytes treated with anti-hTLR2-IgA antibody. Secreted IFN- γ was measured by ELISA in co-cultures of human autologous T cells and monocytes treated with *B. bif*_K57, *B. bif*_K18, *B. bif*_B06 or *B. bif*_R71. Three technical replicates were performed. *P* values were calculated using two-sided unpaired *t*-test. *B. bif*_K57 versus *B. bif*_K57 + TLR2 blocker, *P* = 0.027 (human 3); *B. bif*_K18 versus *B. bif*_K18 + TLR2 blocker, *P* = 0.018 (human 3); *B. bif*_K57 versus *B. bif*_K57 + TLR2 blocker, *P* = 0.0004 (human 4); *B. bif*_K18 versus *B. bif*_K18 + TLR2 blocker, *P* = 0.002 (human 4). **g**, Growth curves of subcutaneous MC38 tumours in *Tlr2* KO mice. *n* = 5 per group. For all graphs, data show the mean \pm s.e.m.; ***P* < 0.01, *****P* < 0.001.

apoptosis of CD8⁺ T cells^{30,31}. Therefore, the decrease in TNF- α levels is suggestive of an enhanced antitumour effect.

We also found that a single treatment of *B. bifidum* inhibited tumour growth (Fig. 2b,c), increased CD4⁺ T, CD8⁺ T and NK cells, and decreased T_{reg} cells in the tumour and spleen (Supplementary Figs. 1–3). In the metabolomics analysis, a single *B. bifidum* treatment increased serum L-tryptophan (Fig. 3b) and induced IFN- γ production from activated CD8⁺ T cells (Fig. 3c). Furthermore, the lipidomics analysis showed that a single treatment with a synergistic *B. bifidum* strain decreased serum lipids levels (Extended Data Fig. 3c). These results demonstrate that a single *B. bifidum* treatment increased antitumour immunity in a different way to that of anti-PD-1.

In our WGS analysis of *B. bifidum*, two non-synergistic strains (*B. bif_B06* and *B. bif_R71*) showed approximately 99.9% nucleotide identity (Fig. 4a), which demonstrates the limitation in representing the diversity of strains in human gut. However, 24 different single nucleotide polymorphisms (SNPs) were identified between the two strains (Supplementary Table 12), and 17 genes (nine *B. bif_B06* genes and eight *B. bif_R71* genes) were detected in only one of the strains (Fig. 4b), which were not detected by repeated WGS of the same bacteria after continuous culturing. Because these similar two strains showed similar non-synergistic effects with the anti-PD-1 antibody, the function of the genes that are affected by the SNPs is not associated with cancer immunity and needs to be further investigated.

Methods

Patient cohort and characteristics. Healthy controls ($n = 154$) underwent a medical check-up at Seoul National University Hospital (SNUH) between February 2017 and June 2017; none had a serious illness at the time of examination. Healthy controls who underwent antibiotic ($n = 4$) or probiotic ($n = 11$) treatment within 3 months before the stool collection were excluded from the study. Patients enrolled in this study were diagnosed with stage IIIB or IV NSCLC through the standardized review performed by expert pathologists at Samsung Medical Center (SMC) between January 2016 and August 2017 ($n = 98$). Patients were excluded from the study if they received antibiotic or probiotic treatment within 3 months before the stool collection. Stool samples from patients were collected before treatment with either platinum-based chemotherapy, EGFR TKI or an immune checkpoint inhibitor. Two patients whose stool samples were collected after the EGFR TKI treatment were excluded. Treatment responses were classified according to the RECIST, v.1.1 (ref. 12). We assessed the objective response in target lesions and classified patients as responders (those experiencing PR) or non-responders (those experiencing SD or PD). All samples were obtained with informed consent at the SMC and SNUH, and the study was approved by the institutional review board in accordance with the Declaration of Helsinki (2008-06-033 and 1609-051-790, respectively).

Stool sample collection and DNA preparation. Healthy controls and patients with NSCLC were requested to self-sample their stool following detailed printed instructions. Collected samples were immediately stored in the freezer (-20°C) for 1 day and transferred in a provided cooler to our facilities, where they were stored at -80°C . DNA extractions were performed on 500 mg of faeces per sample using a FastDNA SPIN kit for soil (MP Biomedicals) according to the manufacturer's instructions. DNA purity and quantity were estimated using a NanoDrop One Spectrophotometer (Thermo Fisher Scientific).

Metagenomic 16S rRNA PCR amplification and sequencing. The V3–V4 region of the bacterial 16S rRNA gene was amplified according to the Illumina 16S Metagenomic Sequencing Library Preparation guide (Illumina) using the following primers with added adapter overhang sequences³²: forward, 5'-TCGTCGGCAGCGTCAGATGTGATAAGAGACAGCCTACGGGNGGCWGCAG-3'; reverse, 5'-GTCTCGTGGGCTCGGAGATGTGATAAGAGACAGGACTACHVGGGTATCTAATCC-3'. The PCRs were performed in a final reaction volume of 25 μl containing 2 μl of genomic DNA ($10\text{ ng } \mu\text{l}^{-1}$), 0.5 μl of each primer (10 μM), 12.5 μl of 2 \times KAPA HiFi HotStart ReadyMix (Kapa Biosystems) and 9.5 μl of distilled water. The following PCR conditions were used: initial denaturation at 95°C for 3 min; 25 cycles of denaturation (95°C for 30 s), annealing (55°C for 30 s) and extension (72°C for 30 s); and final extension at 72°C for 5 min. The PCR products were purified with AMPure XP Beads (Beckman Coulter). Dual indices and Illumina sequencing adapters were attached using 5 μl of the amplicon DNA, 5 μl of Illumina Nextera XT Index Primer 1 (N7xx), 5 μl of Nextera XT Index Primer 2 (S5xx), 25 μl of 2 \times KAPA HiFi HotStart Ready Mix and 10 μl of

nuclease-free water. The following PCR conditions were used: 95°C for 3 min; 8 cycles of 95°C for 30 s, 55°C for 30 s and 72°C for 30 s; and final extension at 72°C for 5 min. PCR products were purified with AMPure XP beads, and quality control of constructed 16S metagenomic libraries was performed using a 2100 Bioanalyzer (Agilent). Libraries were normalized and pooled for sequencing on a MiSeq platform (Illumina) using 2 \times 300 bp paired-end sequencing.

Metagenomic 16S rRNA sequencing and qPCR analysis. The quality control of raw sequences from each sample was performed using FastQC³³. Primer sequences were removed using cutadapt (v.2.2)³⁴. Trimmed sequences were processed using QIIME2 (v.2019.4)³⁵. The DADA2 software package³⁶ wrapped in QIIME2 was used for quality control, including quality filtering, denoising, paired-end sequence merging, chimera filtering and feature tables construction containing amplicon sequence variants. The phylogenetic tree was constructed using the QIIME2 phylogeny plugin (q2-fragment-insertion). α -diversity and β -diversity were analysed using core-metrics-phylogenetic in the QIIME2 diversity plugin. α -diversity and β -diversity significance were calculated using alpha- and beta-group-significance in the QIIME2 diversity plugin, respectively. Taxonomic annotation was performed using the QIIME2 feature-classifier plugin (classify-sklearn) with a pre-trained Naive Bayes classifier on the GreenGene database (v.13.8 with 99% similarity operational taxonomic units)³⁷. The LefSe³⁸ was performed and linear discriminant analysis (LDA) scores were used to identify differential features at the species level between groups. The abundance of *B. bifidum* was determined using a qPCR assay with *B. bifidum*-specific primers and normalized to 16S rRNA-specific results³⁹. TaqMan Fast Advanced Master Mix (Applied Biosystems) and the StepOnePlus real-time PCR system (Applied Biosystems) was used for qPCR experiments. Bacterial primer sequences were as follows: *B. bifidum*, 5'-CTTGAGACCCGCATCGTAT-3' (forward), 5'-ACGTCGGTGGTGAAGAAGTC-3' (reverse) and 5'-FAM-TCTGATCGCGGAGCGCTTCA-BHQ1-3' (probe); 16S rRNA, 5'-AGAGTTTGATCCTGGCTCAG-3' (forward), 5'-CTGCTGCTYCCGTA-3' (reverse) and 5'-FAM-TAACACATGCAAGTCGA-BHQ1-3' (probe).

Shotgun metagenomics sequencing and data analysis. DNA was subjected to 151-bp paired-end sequencing on an Illumina HiSeq 4000 platform. Libraries were prepared using a TruSeq Nano DNA kit (Illumina). All sequencing reads were trimmed for quality control and filtered for host contamination using KneadData v.0.5.4 with default parameters and the human reference database (hg37) built using the script "kneaddata_database --download human bowtie2" (<https://bitbucket.org/biobakery/kneaddata/wiki/Home>). Whole-genome shotgun sequencing data from human stool samples were taxonomically profiled using metagenomic phylogenetic analysis (MetaPhlan2) and functionally profiled using the HUMAnN2 with default parameters^{40,41}. Gene family abundance data from the HUMAnN2 results were analysed using the statistical analysis of metagenomic profiles (STAMP) software⁴²; statistical evaluation was performed using Welch's *t*-test.

Cell culture. The MC38 cell line was purchased from Kerfast (EZH204). The LLC1 cell line was purchased from the American Type Culture Collection (ATCC, CRL1642), as was the 4T1 cell line (ATCC, CRL-2539). For the orthotopic lung cancer model, LLC cells expressing an enhanced firefly luciferase (*effluc*) gene were a gift from Y. H. Jeon (DGMIF, Korea). All cell lines were authenticated using DNA fingerprint analysis and were negative for mycoplasma contamination. Cells were cultured in DMEM (Gibco) with 10% fetal bovine serum (Gibco) and 100 units per ml of penicillin (Gibco) and streptomycin (Gibco). All cells were maintained in a humidified incubator at 37°C in a 5% CO_2 atmosphere.

Mice. All animal experiments were carried out in accordance with protocols approved by the Institutional Animal Care and Use Committee of CHA University, the Gwangju Institute of Science and Technology Animal Care and Use Committee and the DGMIF. All animals used in this study were maintained and handled according to the approved policies of the study protocols. The number of mice assigned to bacteria administration provide sufficient statistical results, including for tumour size and cytokine and immune profiling. All in vivo studies were not blinded, and mice were chosen at random for each group before administration of *B. bifidum* strains. Wild-type C57B6/N (female) and BALB/c (female) mice were provided by Orient Bio. For syngeneic tumour mouse models, female C57B6/N mice (wild-type, 6 weeks old) were given oral doses of *B. bifidum* strains starting 2 weeks before tumour inoculation, and the administration of bacteria continued throughout the experimental period. Mice were subcutaneously injected with 2×10^5 MC38 colon cancer cells. Tumour size was measured three times a week until the end point, and the tumour volume was calculated as $\text{length} \times \text{width}^2 \times 0.5$. After tumour inoculation, the tumour-bearing mice were also intraperitoneally injected with 3 mg per kg oxaliplatin (S1224, Selleckchem) or 2 mg per kg anti-PD-1 monoclonal antibody (mAb; clone RMP1-14, BioXCell) in PBS on days 3, 7, 10, 14, 17 and 21. For the anti-PD-1-resistant syngeneic tumour mouse model, 14 days after the initial oral administration of *B. bif_K57*, female C57B6/N mice (wild type, 6 weeks old) were subcutaneously injected with 5×10^5 LLC1 cells (ATCC, CRL-1642), and 20 mg per kg anti-PD-1 mAb (clone RMP1-14, BioXCell) was

administered via intraperitoneal injection eight times, twice a week, for 28 days. Female BALB/c mice (wild type, 6 weeks old) were subcutaneously injected with 3×10^5 4T1 breast cancer cells (ATCC, CRL-2539). The 4T1 tumour-bearing mice were intraperitoneally injected with 10 mg per kg anti-PD-1 mAb (clone RMP1-14, BioXCell) in PBS on days 3, 7, 10, 14, 17 and 21 after tumour inoculation. For the antibiotics model, female C57B6/N mice (wild type, 6 weeks old) were treated with the ABX antibiotic cocktail consisting of vancomycin (Sigma-Aldrich, V2002, 500 mg per litre), colistin sulfate salt (Sigma-Aldrich, C4461, 6,000 U per ml), ampicillin (Sigma-Aldrich, A1593, 1 g per litre) and neomycin (Sigma-Aldrich, N6386, 1 g per litre) by supplementing it in the drinking water. The ABX-containing water was changed daily and was administered for 2 weeks. For the IFN- γ -neutralization experiment, female C57B6/N mice (wild type, 6 weeks old) were intraperitoneally injected with an anti-mouse IFN γ R mAb (clone GR-20, BioXCell, BE0029) at a concentration of 50 μ g per mouse for three times (once a day; one injection for every 5 days starting the day after tumour cell inoculation). C57BL/6 background *Tlr2* KO mice (7–8 weeks, female) were purchased from The Jackson Laboratory. At 14 days after the oral administration of *B. bif_K57*, *Tlr2* KO mice were subcutaneously injected with 2×10^5 MC38 colon cancer cells and 2 mg per kg anti-PD-1 mAb (clone RMP1-14, BioXCell) or rat IgG2a isotype control (clone 2A3, BioXCell, BE0089) in PBS on days 3, 7, 10, 14, 17, 21 and 23.

Extraction of mouse stool RNA and DNA and qPCR analysis. Total RNA was extracted from mouse stool using a Quick-RNA Faecal/Soil Microbe Microprep kit (R2040, Zymo Research). Complementary DNA was synthesized from the extracted RNA using TOPscriptRT DryMIX (dT18 plus) (RT200, Enzymomics). Expression levels of *RecA*, *MurE* and *GlmM* were measured by PCR with reverse transcription (RT-PCR) using a CFX384 Touch (Bio-Rad). Primer sequences were as follows: *RecA*, 5'-TGCAACGTGGTCAAGAAGTC-3' and 5'-GTGATCTGCGGATTGTCCTT-3'; *MurE*, 5'-GTCGACTACGCGCACACA-3' and 5'-ATGAAGCTGTCAATGCGATG-3'; *GlmM*, 5'-AAGGACATGGCATCAAGAC-3' and 5'-ATTTGACGACTCGTTGCAC-3'. Stool DNA was extracted using a FastDNA SPIN kit for soil (MP Biomedicals). The abundance of *B. bifidum* was determined using a qPCR assay with *B. bifidum*-specific primers and normalized to 16S rRNA-specific results⁵⁹.

Bacterial transplantation and peptidoglycan validation. *B. bif_K57* and *B. bif_K18* were purchased from the Korea Collection for Type Cultures (KCTC). *B. bif_B06* was purchased from DuPont. *B. bif_R71* was purchased from Lallemand. *B. bif_M31* was donated by Mediogen. *B. bif_C01* was donated by ChongKunDang. *B. bifidum* strains were cultured in BL medium at 37°C for 48 h under anaerobic conditions. After each *B. bifidum* strain was cultured, the bacteria were lyophilized for preservation. Next, we checked the colony-forming unit (c.f.u.) counts of lyophilized bacteria. The c.f.u. was measured using a PBS serial dilution method (Corning, 21-040-CVR). For each sampling point, an aliquot of cultured bacteria was diluted to 10^{-6} , 10^{-7} and 10^{-8} , and 100 μ l was spread on a BL agar plate. After c.f.u. counting, each *B. bifidum* strain was divided and sealed into daily administration doses and stored at 4°C. Each *B. bifidum* strain was suspended in PBS at a concentration of 5×10^9 c.f.u. per ml. During the experiment, each mouse was given 200 μ l of probiotics daily by oral gavage. For bacterial peptidoglycan measurement, each *B. bifidum* strain was cultured to 5×10^9 c.f.u. per ml, and sonicated for 10 min (10-s on/20-s off cycle). Peptidoglycan levels were measured using a peptidoglycan ELISA kit (MyBioSource).

Human T-cell response to bacteria. Blood samples were collected from healthy donors with informed consent at the GIST, Korea. The study was approved by the institutional review board (20192009-BR-48-02-04). Peripheral blood mononuclear cells (PBMCs) were purified using Ficoll-Paque Plus (GE Healthcare Life Sciences) density gradient centrifugation. For experiments, *Leuconostoc mesenteroides* GEN3016, *L. mesenteroides* KM20-2 and *Leuconostoc garlicum* KM20-1 were donated by Genome and Company. *B. bifidum* strains were cultured in MRS medium (Kisanbio) at 37°C for 24 h under anaerobic conditions, and *Leuconostoc* strains were cultured in MRS medium at 37°C for 24 h under aerobic conditions. Monocytes were isolated from at least 2×10^6 PBMCs using a Negative Immunomagnetic Selection kit (Miltenyi Biotec) and suspended in RPMI 1640 medium (Gibco/Invitrogen) supplemented with 10% human AB⁺ serum (Sigma-Aldrich) and 1% 2 mmol per litre glutamine (Gibco/Invitrogen). Monocytes were distributed into 96-well plates at 5×10^5 cells per well, and then incubated alone or with *Bifidobacterium* strains or *Leuconostoc* strains at 5×10^4 c.f.u. per ml for 2 h at 37°C under a 5% CO₂ atmosphere. Autologous CD4⁺ or CD8⁺ T cells were isolated from the remaining PBMCs using a Negative Immunomagnetic Selection kit and suspended at 5×10^4 cells per well in RPMI 1640, 10% human AB⁺ serum, 1% 2 mM glutamine, 20 IU per ml IL-2 (Peprotech), 1,000 IU per ml granulocyte-macrophage colony-stimulating factor (Miltenyi Biotec), 1% penicillin-streptomycin (Gibco/Invitrogen) and 50 μ g ml⁻¹ gentamycin (Gibco/Invitrogen). Monocyte-bacteria-T cell co-cultures were incubated for 48 h at 37°C under 5% CO₂. Supernatants were collected and stored at -20°C, and IFN- γ levels were measured using a Human IFN- γ ELISA MAX Deluxe kit (BioLegend). For the TLR2-blocking experiment, monocytes were first co-cultured with 10 μ g ml⁻¹ of anti-hTLR2-IgA antibody (Invivogen) for 1 h at 37°C under 5%

CO₂, and then incubated with microbes at 5×10^4 c.f.u. per ml for 2 h under the same conditions. Autologous CD4⁺ or CD8⁺ T cells were suspended at 5×10^4 cells per well and incubated for 48 h at 37°C under 5% CO₂.

In vitro T-cell IFN- γ production assay. Ninety-six-well plates were coated with 2.5 μ g ml⁻¹ anti-human CD3 antibody (BioLegend, clone OKT3), either alone or with 2.5 μ g ml⁻¹ L-tryptophan (Sigma-Aldrich) in PBS for 4 h at 37°C in a 5% CO₂ atmosphere. Wells were washed three times with PBS before adding purified CD8⁺ T cells (2×10^5 per well) in complete RPMI 1640 medium (10% fetal bovine serum (Gibco), 100 units per ml of penicillin (Gibco) and streptomycin (Gibco), 1% L-glutamine (Gibco) and 0.1% β -mercaptoethanol). After 3 days, supernatant was obtained, and the level of IFN- γ was confirmed by ELISA (Invitrogen).

Orthotopic syngeneic mouse model of lung cancer. Male C57B6/N mice (5 weeks old) were purchased from Orient Bio and housed in a specific-pathogen-free facility at the Laboratory Animal Center, DGMIF, before use. LLCs expressing an enhanced firefly luciferase (*effluc*) gene were donated by Y. H. Jeon (DGMIF, Korea). For in vivo experiments, LLC-*effluc* cells were grown to the exponential phase and then collected by trypsinization. Cells were then washed and resuspended in an ice-cold 50:50 solution of growth-factor-reduced Matrigel (BD Bioscience) and Hank's balanced salt solution (HyClone). Mice were anaesthetized using 2–3% isoflurane and placed in a right lateral decubitus position. A 1-cm skin incision was performed below the left scapula. A volume of 20 μ l of final cell suspension (1×10^6) was injected into the parenchyma of the left lung through the intercostal space to a depth of 3 mm using a 29-gauge needle attached to a 0.5-ml syringe (Becton Dickinson). The skin incision was closed with a surgical skin clip and the mice were observed under a heating lamp until fully recovered. The mouse body weight was measured twice a week. Successful orthotopic injections were confirmed by immediate whole-body bioluminescence imaging.

Bioluminescence imaging. Mice were intraperitoneally administered with firefly D-Luciferin potassium salt (Perkin Elmer) at a dose of 150 mg per kg body weight in DPBS and anaesthetized with 2–3% isoflurane 5 min before the peak luciferin uptake time. Bioluminescence images were acquired using an IVIS Spectrum CT (Perkin Elmer). During image acquisition, anaesthesia was maintained with 2% isoflurane. Determination of the optimal bioluminescence image acquisition time for the orthotopic syngeneic mouse model of lung cancer was assessed using a 30-min dynamic scan. Serial images were obtained from all animals, and the peak signal of photon flux was determined. Analysis was performed using Living Image software by measuring the total photon flux (measured in photon s⁻¹) using a standard rectangular shaped region of interest (same size over all time points) manually drawn over the body of the mouse.

Flow cytometry analysis. FACS sequential gating strategies are provided in Supplementary Figs. 4 and 5. Tumours, spleens and intestines from mice were collected at day 15 after MC38 tumour cell inoculation. Dissected tumours were cut into small pieces and transferred into RPMI 1640 medium (Gibco/Invitrogen) supplemented with 2.5 mg ml⁻¹ collagenase type 1, 1.5 mg ml⁻¹ collagenase type 2, 1 mg ml⁻¹ collagenase type 4, 50 μ g ml⁻¹ DNase type 1 and 0.25 mg ml⁻¹ hyaluronidase type IV-S. The samples were incubated for 50 min at 37°C, and then filtered through a 70- μ m cell strainer (BD Bioscience). The spleens were mashed in RPMI 1640 medium, incubated in RBC lysis buffer (eBioscience) and filtered through a 70- μ m cell strainer. Lamina propria cells were isolated from the large intestine according to a previously described isolation protocol⁶⁰. To block the Fc receptor, spleen, tumour and lamina propria cells were incubated with anti-mouse CD16/CD32 (BD Bioscience) for 10 min at 4°C. After viability and surface staining, fixation/permeabilization buffer set (BioLegend) solution was added. The following anti-mouse antibodies were used for spleen and tumour immune cell profiling: CD45 (1:100 dilution; BioLegend, 103116); CD3 (1:20 dilution; BioLegend, 100218); NK1.1 (1:100 dilution; BioLegend, 108708); CD49b (1:100 dilution; BioLegend, 108910); CD4 (1:100 dilution; BioLegend, 100422); CD25 (1:20 dilution; BioLegend, 101904); FOXP3 (1:20 dilution; Invitrogen, 17-5773-82); CD44 (1:100 dilution; BioLegend, 103008); CD62L (1:100 dilution; BioLegend, 104412); CD8a (1:25 dilution; BioLegend, 100706, spleen and tumour); CD8a (1:80 dilution; BioLegend, 100712, intestine cytokine expression); IFN- γ (1:50 dilution; BioLegend, 505806); and IL-2 (1:200 dilution; BioLegend, 503820). Stained cell acquisition was performed with CANTO II (BD Bioscience) using BDFACS Diva software v.8.0.2 (BD Bioscience), and data analysis was performed using FlowJo software (v.10, TreeStar).

Cytokine real-time PCR of tumours. Total RNA was extracted from mouse tumour tissues using a RNeasy Plus Mini kit (Qiagen). Reverse transcription was conducted using a PrimeScript First Strand cDNA Synthesis kit (Takara). Two micrograms of total RNA were reverse-transcribed to synthesize cDNA. Expression levels of *Ifng*, *Tnfa*, *Il2* and *Il10* were measured by RT-PCR using a CFX384 Touch (Bio-Rad). Primer sequences were as follows: *Ifng*, 5'-GAAAGCCTAGAAAGTCTGAATAACT-3' and 5'-ATCAGCAGCGACTCCTTTTCCGCTT-3'; *Tnfa*, 5'-GCCTCTTCTCATTCTGCTTG-3' and 5'-CTGATGAGAGGGAGGCCATT-3'; *Il2*,

5'-ATGTACAGCATGCAGCTCGCATC-3' and 5'-GGCTTGTGAGATG ATGCTTTGACA-3'; *Il10*, 5'-TGAAGACCCTCAGGATGCGG-3' and 5'-AGAG CTCTGTCTAGGTCCTGG-3'; *Actb* (β -actin), 5'-CGTGGGTGACATCA AAGAGAA-3' and 5'-TGGATGCCACAGGATTCAT-3'. PCR was performed in 20- μ l volumes containing 2 μ l of genomic DNA (50 ng μ l⁻¹), 0.4 μ l of each primer (10 μ M), 10.0 μ l of SYBR Premix Ex Taq (Tli RNase H Plus) (Takara) and 7.2 μ l of distilled water. PCR conditions were as follows. For *Irfng*, *Tnfa*, *Il2* and *Actb*: initial denaturation at 95 °C for 1 min; 35 cycles of denaturation (95 °C for 30 s), annealing (60 °C for 30 s) and extension (72 °C for 1 min); and final extension at 72 °C for 1 min. For *Il10*: initial denaturation at 95 °C for 1 min, 40 cycles of denaturation (95 °C for 30 s), annealing (60 °C for 30 s) and extension (72 °C for 1 min); and final extension at 72 °C for 1 min.

Mouse intestine RNA sequencing and data analysis. Mice were killed on day 22 after MC38 tumour cell inoculation, and RNA was extracted from intestinal tissue using a RNeasy Mini kit (Qiagen). Next, 151-bp paired-end libraries were constructed from 1 μ g of RNA using a TruSeq RNA Sample Prep kit v.2 (Illumina). WTS was performed on an Illumina HiSeq instrument. RNA-sequencing reads from each WTS experiment were aligned to the mouse reference genome (GRCm38) using STAR aligner⁴³. Quantification of gene expression and differential expression analysis were performed using RSEM⁴⁵ and the DESeq2 R package⁴⁶. The ClueGO plug-in (v.2.5.4; <http://www.ici.upmc.fr/cluego/>) in Cytoscape software (v.3.3.0; <http://cytoscape.org/>) was used to analyse GO terms⁴⁷. Functionally related GO terms for biological processes in *Mus musculus* (v.27 February 2019) were grouped based on a kappa score > 0.4 with network specificity of 5–10 using GO term fusion. Statistical significance was calculated using a two-sided hypergeometric test, and the FDR was corrected using the Bonferroni step-down method.

Mouse serum lipidomic profiling. Materials and reagents. Thirty-seven lipid standards were utilized to optimize nanoflow ultrahigh performance liquid chromatography–electrospray ionization–tandem–mass spectrometry (nUHPLC–ESI–MS/MS) run conditions: lysophosphatidylcholine (LPC) 16:0; LPC 17:0; phosphatidylcholine (PC) 12:0/12:0; PC 13:0/13:0; PC 16:0/16:0; PC plasmalogen (PCp) 18:0p/22:6; lysophosphatidylethanolamine (LPE) 17:1; LPE 18:0; phosphatidylethanolamine (PE) 14:0/14:0; PE 16:0/16:0; PE 17:0/17:0; PE plasmalogen (PEp) 18:0p/22:6; lysophosphatidic acid (LPA) 17:0; LPA 18:0; phosphatidic acid (PA) 17:0/17:0; PA 14:0/14:0; lysophosphatidylglycerol (LPG) 12:0; LPG 17:1; LPG 18:0; phosphatidylglycerol (PG) 15:0/15:0; PG 16:0/16:0; lysophosphatidylinositol (LPI) 17:1; LPI 18:0; phosphatidylinositol (PI) 16:0/18:1; PI 12:0/13:0; sphingomyelin (SM) d18:0/16:0; SM d18:0/17:0; SM d18:0/18:0; ceramide (Cer) d18:1/14:0; Cer d18:1/17:0; sulfatide (SulfoHexCer) d18:1/17:0; SulfoHexCer d18:1/24:0; monohexosylceramide (HexCer) d18:1/17:0; HexCer d18:1/16:0; diacylglycerol (DG) 17:0/17:0D5; DG 16:0_18:1; and triacylglycerol (TG) 17:0/17:1/17:0D5. All phospholipid (PL) standards were purchased from Avanti Polar Lipids. Lipids with odd-numbered fatty acyl chains were used as internal standards added to the serum sample for quantification using the selected reaction monitoring method. PL standards were diluted to 2 pmol μ l⁻¹ in a binary solvent mixture (CH₃OH:H₂O, 8:2, v/v), and the PL standard mixtures were stored at –10 °C until use. HPLC-grade solvents (H₂O, CH₃CN, CH₃OH, isopropyl alcohol and methyl-tert-butyl ether (MTBE)) were purchased from Avantor Performance Materials. Ammonium hydroxide (NH₄OH), ammonium formate (NH₄HCO₂) and CHCl₃ were purchased from Sigma-Aldrich. Silica capillary tubes (20-, 50- and 100- μ m inner diameter; 360- μ m outer diameter) for capillary liquid chromatography columns were purchased from Polymicro Technologies. Packing materials for the home-made capillary liquid chromatography columns were ethylene bridged hybrid (BEH) particles (1.7 μ m) unpacked from Acquity UHPLC BEH C-18 columns (2.1 mm \times 100 mm) from Waters and Watchers ODS-P C-18 particles (3 μ m and 100 Å) from Isu Industry.

Lipid extraction from mouse serum samples. Mouse serum samples were stored at –80 °C until use. Lipids were extracted with 100- μ l aliquots of each mouse serum sample following the extraction procedure using MTBE/CH₃OH⁴⁸. One-hundred microlitres of each serum sample was dried in a vacuum centrifuge, a model Bondiro MCFD 8508 freeze dryer with a concentrator from Ilshin Lab. To the dried powder, 300 μ l of methanol was added, the sample was incubated in an ice bath for 10 min, 1,000 μ l of MTBE was added and the sample was vortexed for 1 h. For phase separation, 250 μ l of MS-grade water was added to the mixture. The sample was vortexed for 10 min and then centrifuged at 1,000 \times g for 10 min. The supernatant organic solvent layer was transferred to another centrifuge tube, and 300 μ l of MTBE was added to the remaining lower layer. After tip sonication for 2 min followed by centrifugation at 1,000 \times g for 10 min, the organic solvent supernatant layer was retrieved and combined with the previously collected organic layer. The final mixture was dried in a vacuum centrifuge, converting it to an extracted lipid powder. Dried lipids were weighed, re-concentrated at 15 μ g μ l⁻¹ in CHCl₃:CH₃OH (1:9, v/v), and stored at –30 °C. The extracted lipid sample was diluted at 5 μ g μ l⁻¹ in H₂O:CH₃OH (2:8, v/v) for nUHPLC–ESI–MS/MS analysis.

Lipid analysis of mouse serum by nUHPLC–ESI–MS/MS. Lipid analysis was performed in two steps. First, global identification of the lipid molecular structure

of each lipoprotein fraction was performed on a Dionex Ultimate 3000 RSLCnano System coupled with a LTQ Velos ion trap mass spectrometer from Thermo Fisher Scientific. Then, targeted quantitation of identified lipids was performed for individual samples using a model nanoAcquity UPLC system from Waters equipped with a TSQ Vantage triple-stage quadrupole MS system from Thermo Fisher Scientific. Analytical capillary columns were made in the laboratory by pulling one end of the fused silica capillary (100- μ m inner diameter, 360- μ m outer diameter) through a flame to make a sharp needle for the self-emitter for ESI. Before packing the analytical column, a 0.5-cm portion of the column tip was packed with Watchers C-18 particles (3 μ m and 100 Å) to prepare self-assembled frits, and then the remaining 6.5-cm length was packed with BEH resins (7 μ m and 100 Å) under nitrogen gas at 1,000 p.s.i. Mobile phases were H₂O:CH₃CN (9:1, v/v) for A and CH₃OH:CH₃CN:isopropyl alcohol (2:2:6, v/v/v) for B, and both were added with a mixture of ionization modifiers (5 mM NH₄HCO₂ and 0.05 % NH₄OH), which was used in positive and negative ion modes. While the samples were loading, 100% of mobile phase A was delivered to the analytical column at 730 nl min⁻¹ for 12 min with the split valve closed. In positive-ion mode, gradient elution began with 75% of mobile phase B, which was increased to 80% for 2 min at a pump flow rate of 7.5 μ l min⁻¹ with the split valve on so that only 300 nl min⁻¹ of flow was delivered to the analytical column. Mobile phase B was maintained at 80% for 8 min, ramped continuously to 85% for 15 min, and then ramped to 100% for 10 min. Finally, 100% of mobile phase B was maintained for 10 min to wash the column. Then, mobile phase B was returned to 0% over 5 min to recondition the analytical column. In negative-ion mode, gradient elution began with 75% B, which was ramped to 85% for 5 min, 88% for 8 min and 100% for 14 min. Finally, mobile phase B was maintained at 100% for 10 min to wash the column. The column was then reconditioned as described above. The *m/z* range for the precursor scan was 250–1,200, and 40% of normalized collision energy was applied to collision-induced dissociation experiments. The ESI voltage applied was 3 kV for both positive- and negative-ion modes. Identification of lipid structures was performed by LipiPilot, a software package designed to determine the lipid molecular structure from a collision-induced dissociation spectra program⁴⁹.

Targeted quantitation of identified lipids in individual samples was performed by nUHPLC–ESI–MS/MS, based on the selected reaction monitoring method, using the analytical column. Quantitation of identified lipids was performed using gradient conditions optimized to achieve high speed separation. Sample loading (5 μ g μ l⁻¹ of lipid extracts mixed with 1 pmol of each of the 16 internal standards) was performed at 0.8 μ l min⁻¹ for 10 min. An applied gradient elution condition began at 75% of the mobile phase B, which was increased to 80% for 5 min, 90% for 9 min and 100% for 10 min to wash the column. Then, mobile phase B was returned to 0% for 5 min to recondition the column. Detection of ions was accomplished in the polarity-switching mode (positive and negative ion modes alternately) with the scan width at *m/z* 1.0, the scan time at 0.001 s and an ESI voltage of 3 kV for quantitation. LPC, PC, PCp, LPE, PE, PEp, SM, Cer, HexCer, SulfoHexCer, DG and TG were detected in positive-ion mode, and LPG, PG, LPI, PI, LPA and PA were detected in negative-ion mode.

Mouse serum metabolome profiling. UPLC–Q–TOF/MS analysis. Four volumes of 80% methanol in water were added to 20 μ l of serum. After vortexing for 1 h at room temperature, the mixtures were centrifuged at 13,000 \times g for 20 min at 4 °C. The supernatant was transferred to a sample vial and injected into an UPLC–quadrupole time-of-flight mass spectrometry (UPLC–Q/TOF–MS; Synapt G2Si, Waters) system. UPLC separation was performed using an Acquity UPLC BEH C18 column (2.1 mm \times 100 mm, 1.7 μ m, Waters). Mobile phase A consisted of 0.1% formic acid in water, whereas mobile phase B consisted of 0.1% formic acid in CH₃CN. Samples were eluted using the following conditions: initial 0% B to 5% at 1 min, to 95% B at 9 min, to 100% B at 10.5 min, to 0% B at 11 min, with equilibration for an additional 1.5 min. The flow rate was 0.4 ml min⁻¹, and the column temperature was maintained at 40 °C. Mass acquisition was performed in both positive and negative ESI modes with the following parameters: capillary voltage of 2.0 kV; cone voltage of 10 V; source temperature of 110 °C; desolvation temperature of 400 °C; and desolvation gas flow of 650 litres per h. Mass data were collected in the range *m/z* 60–1,400, with a scan time of 0.25 s and an inter-scan time of 0.02 s for 12 min. Mass data, including retention time, *m/z* and ion intensities, were extracted using Progenesis Q1 software (Waters).

For metabolite identification, the following resources were used: exact mass, molecular formula suggested by MassLynx software (Waters) based on element and isotope composition of the parent mass ion; MS/MS spectra of the compounds; and metabolome databases, including the Human Metabolomics Database (<http://www.hmdb.ca/>), METLIN (<http://metlin.scripps.edu/>), MASS Bank (<http://www.massbank.jp/>)⁵⁰ and LIPID MAPS (<http://www.lipidmaps.org/>)⁵¹. Wilcoxon–Mann–Whitney *U*-tests were used to compare the relative abundance of L-tryptophan between the groups. A *P* value less than 0.05 was considered statistically significant.

Bacterial whole-genome shotgun sequencing and data analysis for *Bifidobacterium* strains. Bacterial DNA was extracted using a Quick-DNA fungal/bacterial kit (Zymo Research) from each sample and subjected to 101-bp paired-end sequencing using an Illumina HiSeq 2500. Libraries were prepared

using a TruSeq Nano DNA kit (Illumina). All sequencing reads were trimmed for quality using BBduk (hdist=1 minlen=50 qtrim=rl trimq=20 ktrim=r k=23 mink=11 tpe tbo) from the BBmap package (v.38.34; <http://sourceforge.net/projects/bbmap/>). Trimmed reads were assembled using SPAdes with default parameters in careful mode (v.3.10.1)⁵². Contigs from SPAdes output (contigs.fasta) were filtered out by a contig coverage cut-off of 10 and a length cut-off of 100 bases. The assembly quality was checked using QUAST with default parameters (v.4.5)⁵³ and annotated using Prokka with default parameters (v.1.12)⁵⁴. The pan-genome of the five *Bifidobacterium* strains was identified using Roary with -e and -n (--mafft) parameters (v.3.11.2) to determine the core and accessory genes⁵⁵. ANI scores were calculated using the script of average_nucleotide_identity.py in pyani (v.0.2.9) with -m ANIm and -g parameters⁵⁶. Venn diagrams representing the number of shared and exclusive genes between the *B. bifidum* strains were drawn using jvarkit (v.1.9)⁵⁷. The contig and coverage information of sequencing are provided in Supplementary Tables 7 and 13. BactSNP was used with default parameters to identify SNPs among bacterial isolates with the *B. bifidum* (GCF_001020275.1) genome as a reference.

Bacterial RNA sequencing and data analysis. We performed transcriptome sequencing of the *B. bifidum* strains in their exponential phase. *B. bifidum* strains were cultured in BL agar medium at 37 °C for 48 h under anaerobic conditions. After colony isolation from the BL agar plate, the colony was cultured in BL broth medium at 37 °C for 48 h under anaerobic conditions. Subsequently, the broth medium was centrifuged and the supernatant was removed. Bacterial RNA was extracted using a ZymoBIOMICS RNA Miniprep kit (Zymo Research). rRNA was removed using a Ribo-Zero rRNA Removal kit (Bacteria) (Epicentre). Libraries were prepared using a TruSeq RNA Sample Prep kit v.2 (Illumina), and 101-bp paired-end sequencing was performed on an Illumina HiSeq 2500. RNA-sequencing reads were mapped to the pan-genome of *B. bifidum* using READemption pipeline (v.0.4.3)⁵⁸. Read counts were quantified using the subcommand “gene_quant” of READemption. Differential gene expression analysis was performed with DESeq2 (ref. ⁴⁶) using the subcommand “deseq” of READemption and the edgeR package⁵⁹. A functionally grouped annotation network for the selected genes was constructed using the Cytoscape plugin ClueGO (v.2.5.4)⁵⁷. For *B. bifidum*, functionally related GO terms for biological processes in *Bacillus cereus* ATCC 14579 (v.2 May 2019) were grouped based on a kappa score > 0.4 with network specificity of 3–8 using GO term fusion.

Statistics and reproducibility. Sample sizes and statistical methods are provided in the figure legends. Statistical calculations were performed using Prism (v.8.4.3, GraphPad) and Rex (v.3.4.0, RexSoft). Differences between two variables and multiple variables were assessed by Mann–Whitney *U*-test, Student’s *t*-test and analysis of variance (ANOVA) with Tukey’s multiple comparison test, respectively. Associations between two discrete variables were estimated by Fisher’s exact test. The differences were considered significant if the *P* value was lower than 0.05. All studies are representative of two or more independent experiments, unless indicated otherwise. All tests were successfully replicated.

Reporting Summary. Further information on research design is available in the Nature Research Reporting Summary linked to this article.

Data availability

16S rRNA and WGS data from human stool samples, the mouse intestinal RNA sequencing data, the bacterial WGS data and the bacterial RNA sequencing data have been deposited in the European Nucleotide Archive (accession number PRJEB26531). Source data are provided with this paper.

Received: 5 January 2020; Accepted: 13 November 2020;

Published online: 11 January 2021

References

- Viaud, S. et al. The intestinal microbiota modulates the anticancer immune effects of cyclophosphamide. *Science* **342**, 971–976 (2013).
- Daillère, R. et al. *Enterococcus hirae* and *Barnesiella intestinihominis* facilitate cyclophosphamide-induced therapeutic immunomodulatory effects. *Immunity* **45**, 931–943 (2016).
- Iida, N. et al. Commensal bacteria control cancer response to therapy by modulating the tumor microenvironment. *Science* **342**, 967–970 (2013).
- Sivan, A. et al. Commensal *Bifidobacterium* promotes antitumor immunity and facilitates anti-PD-L1 efficacy. *Science* **350**, 1084–1089 (2015).
- Gopalakrishnan, V. et al. Gut microbiome modulates response to anti-PD-1 immunotherapy in melanoma patients. *Science* **359**, 97–103 (2018).
- Thaiss, C. A., Zmora, N., Levy, M. & Elinav, E. The microbiome and innate immunity. *Nature* **535**, 65–74 (2016).
- Honda, K. & Littman, D. R. The microbiota in adaptive immune homeostasis and disease. *Nature* **535**, 75–84 (2016).
- Rosshart, S. P. et al. Wild mouse gut microbiota promotes host fitness and improves disease resistance. *Cell* **171**, 1015–1028 (2017).
- Vétizou, M. et al. Anticancer immunotherapy by CTLA-4 blockade relies on the gut microbiota. *Science* **350**, 1079–1084 (2015).
- Routy, B. et al. Gut microbiome influences efficacy of PD-1-based immunotherapy against epithelial tumors. *Science* **359**, 91–97 (2018).
- Matson, V. et al. The commensal microbiome is associated with anti-PD-1 efficacy in metastatic melanoma patients. *Science* **359**, 104–108 (2018).
- Eisenhauer, E. A. et al. New response evaluation criteria in solid tumours: revised RECIST guideline (version 1.1). *Eur. J. Cancer* **45**, 228–247 (2009).
- Guerrero-Ros, I. et al. The negative effect of lipid challenge on autophagy inhibits T cell responses. *Autophagy* **16**, 223–238 (2020).
- Gao, J. et al. Loss of IFN- γ pathway genes in tumor cells as a mechanism of resistance to anti-CTLA-4 therapy. *Cell* **167**, 397–404.e9 (2016).
- Patel, S. J. et al. Identification of essential genes for cancer immunotherapy. *Nature* **548**, 537–542 (2017).
- Medzhitov, R. Toll-like receptors and innate immunity. *Nat. Rev. Immunol.* **1**, 135–145 (2001).
- Kohwi, Y., Imai, K., Tamura, Z. & Hashimoto, Y. Antitumor effect of *Bifidobacterium infantis* in mice. *GANN* **69**, 613–618 (1978).
- Rafter, J. Probiotics and colon cancer. *Best. Pract. Res. Clin. Gastroenterol.* **17**, 849–859 (2003).
- Zhang, L. S. & Davies, S. S. Microbial metabolism of dietary components to bioactive metabolites: opportunities for new therapeutic interventions. *Genome Med.* **8**, 46 (2016).
- Desbonnet, L., Garrett, L., Clarke, G., Bienenstock, J. & Dinan, T. G. The probiotic *Bifidobacteria infantis*: an assessment of potential antidepressant properties in the rat. *J. Psychiatr. Res.* **43**, 164–174 (2008).
- Xiao, J. et al. Effects of milk products fermented by *Bifidobacterium longum* on blood lipids in rats and healthy adult male volunteers. *J. Dairy Sci.* **86**, 2452–2461 (2003).
- An, H. M. et al. Antiobesity and lipid-lowering effects of *Bifidobacterium* spp. in high fat diet-induced obese rats. *Lipids Health Dis.* **10**, 116 (2011).
- Wang, K. et al. *Bifidobacterium bifidum* TMC3115 can characteristically influence glucose and lipid profile and intestinal microbiota in the middle-aged and elderly. *Probiotics Antimicrob. Proteins* **11**, 1182–1194 (2019).
- Howie, D., Ten Bokum, A., Necula, A. S., Cobbold, S. P. & Waldmann, H. The role of lipid metabolism in T lymphocyte differentiation and survival. *Front. Immunol.* **8**, 1949 (2018).
- Long, J. et al. Lipid metabolism and carcinogenesis, cancer development. *Am. J. Cancer Res.* **8**, 778–791 (2018).
- Cruceri, D., Baldasici, O., Balacescu, & Berindan-Neagoe, I. The dual role of tumor necrosis factor- α (TNF- α) in breast cancer: molecular insights and therapeutic approaches. *Cell. Oncol.* **43**, 1–18 (2020).
- Chen, X., Bäuml, M., Männel, D. N., Howard, O. Z. & Oppenheim, J. J. Interaction of TNF with TNF receptor type 2 promotes expansion and function of mouse CD4⁺ CD25⁺ T regulatory cells. *J. Immunol.* **179**, 154–161 (2007).
- Schioppa, T. et al. B regulatory cells and the tumor-promoting actions of TNF- α during squamous carcinogenesis. *Proc. Natl Acad. Sci. USA* **108**, 10662–10667 (2011).
- Zhao, X. et al. TNF signaling drives myeloid-derived suppressor cell accumulation. *J. Clin. Invest.* **122**, 4094–4104 (2012).
- Zheng, L. et al. Induction of apoptosis in mature T cells by tumour necrosis factor. *Nature* **377**, 348–351 (1995).
- Bertrand, F. et al. Blocking tumor necrosis factor α enhances CD8 T-cell-dependent immunity in experimental melanoma. *Cancer Res.* **75**, 2619–2628 (2015).
- Klindworth, A. et al. Evaluation of general 16S ribosomal RNA gene PCR primers for classical and next-generation sequencing-based diversity studies. *Nucleic Acids Res.* **41**, e1 (2013).
- Davis, M. P., van Dongen, S., Abreu-Goodger, C., Bartonicek, N. & Enright, A. J. Kraken: a set of tools for quality control and analysis of high-throughput sequence data. *Methods* **63**, 41–49 (2013).
- Martin, M. Cutadapt removes adapter sequences from high-throughput sequencing reads. *EMBnet.journal* **17**, 10–12 (2011).
- Bolyen, E. et al. Reproducible, interactive, scalable and extensible microbiome data science using QIIME 2. *Nat. Biotechnol.* **37**, 852–857 (2019).
- Callahan, B. J. et al. DADA2: high-resolution sample inference from Illumina amplicon data. *Nat. Methods* **13**, 581–583 (2016).
- DeSantis, T. Z. et al. Greengenes, a chimera-checked 16S rRNA gene database and workbench compatible with ARB. *Appl. Environ. Microbiol.* **72**, 5069–5072 (2006).
- Segata, N. et al. Metagenomic biomarker discovery and explanation. *Genome Biol.* **12**, R60 (2011).
- Hill, D. A. et al. Metagenomic analyses reveal antibiotic-induced temporal and spatial changes in intestinal microbiota with associated alterations in immune cell homeostasis. *Mucosal Immunol.* **3**, 148–158 (2010).
- Segata, N. et al. Metagenomic microbial community profiling using unique clade-specific marker genes. *Nat. Methods* **9**, 811–814 (2012).

41. Abubucker, S. et al. Metabolic reconstruction for metagenomic data and its application to the human microbiome. *PLoS Comput. Biol.* **8**, e1002358 (2012).
42. Parks, D. H., Tyson, G. W., Hugenholtz, P. & Beiko, R. G. STAMP: statistical analysis of taxonomic and functional profiles. *Bioinformatics* **30**, 3123–3124 (2014).
43. Ferrer-Font, L. et al. High-dimensional analysis of intestinal immune cells during helminth infection. *eLife* **9**, e51678 (2020).
44. Dobin, A. et al. STAR: ultrafast universal RNA-seq aligner. *Bioinformatics* **29**, 15–21 (2013).
45. Li, B. & Dewey, C. N. RSEM: accurate transcript quantification from RNA-seq data with or without a reference genome. *BMC Bioinformatics* **12**, 323 (2011).
46. Love, M. I., Huber, W. & Anders, S. Moderated estimation of fold change and dispersion for RNA-seq data with DESeq2. *Genome Biol.* **15**, 550 (2014).
47. Bindea, G. et al. ClueGO: a Cytoscape plug-in to decipher functionally grouped gene ontology and pathway annotation networks. *Bioinformatics* **25**, 1091–1093 (2009).
48. Bang, D. Y., Byeon, S. K. & Moon, M. H. Rapid and simple extraction of lipids from blood plasma and urine for liquid chromatography–tandem mass spectrometry. *J. Chromatogr. A* **1331**, 19–26 (2014).
49. Lim, S., Byeon, S. K., Lee, J. Y. & Moon, M. H. Computational approach to structural identification of phospholipids using raw mass spectra from nanoflow liquid chromatography–electrospray ionization–tandem mass spectrometry. *J. Mass Spectrom.* **47**, 1004–1014 (2012).
50. Horai, H. et al. MassBank: a public repository for sharing mass spectral data for life sciences. *J. Mass Spectrom.* **45**, 703–714 (2010).
51. Ivanova, P. T., Milne, S. B., Myers, D. S. & Brown, H. A. Lipidomics: a mass spectrometry based systems level analysis of cellular lipids. *Curr. Opin. Chem. Biol.* **13**, 526–531 (2009).
52. Bankevich, A. et al. SPAdes: a new genome assembly algorithm and its applications to single-cell sequencing. *J. Comput. Biol.* **19**, 455–477 (2012).
53. Gurevich, A., Saveliev, V., Vyahhi, N. & Tesler, G. QUAST: quality assessment tool for genome assemblies. *Bioinformatics* **29**, 1072–1075 (2013).
54. Seemann, T. Prokka: rapid prokaryotic genome annotation. *Bioinformatics* **30**, 2068–2069 (2014).
55. Page, A. J. et al. Roary: rapid large-scale prokaryote pan genome analysis. *Bioinformatics* **31**, 3691–3693 (2015).
56. Pritchard, L., Glover, R. H., Humphris, S., Elphinstone, J. G. & Toth, I. K. Genomics and taxonomy in diagnostics for food security: soft-rotting enterobacterial plant pathogens. *Anal. Methods* **8**, 12–24 (2016).
57. Bardou, P., Mariette, J., Escudié, F., Djemiel, C. & Klopp, C. jvenn: an interactive Venn diagram viewer. *BMC Bioinformatics* **15**, 293 (2014).
58. Förstner, K. U., Vogel, J. & Sharma, C. M. READemption—a tool for the computational analysis of deep-sequencing-based transcriptome data. *Bioinformatics* **30**, 3421–3423 (2014).
59. Robinson, M. D., McCarthy, D. J. & Smyth, G. K. edgeR: a Bioconductor package for differential expression analysis of digital gene expression data. *Bioinformatics* **26**, 139–140 (2010).

Acknowledgements

This research was supported by the Bio & Medical Technology Development Program of the National Research Foundation (NRF), funded by the Ministry of Science & ICT

(NRF-2017M3A9F3046536 to H.P.); a GIST Research Institute (GRI) grant, funded by the GIST in 2020; Genome and Company (grant number GNC GR 17-01 to H.P.). This work was also supported by grants from National Cancer Centre, Korea (NCC-1911267 to H.P.); the Post-Genome Technology Development Program (10067758, Business model development driven by clinico-genomic database for precision immuno-oncology to S.-H.L.) funded by the Ministry of Trade, Industry and Energy (MOTIE, Korea). S.-Y.C. is supported by the Bio & Medical Technology Development Program of the NRF, funded by the Ministry of Science & ICT (NRF-2018M3A9F3056902). This research was also supported by a grant from the Korea Health Technology R&D Project through the Korea Health Industry Development Institute (KHIDI), funded by the Ministry of Health & Welfare, Republic of Korea (grant number H117C1076 to K.W.Y.). This work was supported by the NRF grant funded by the Korea government (MSIT) (number 2017R1C1B2011196 to K.W.Y.). M.H.M. is supported by grant NRF-2018R1A2A1A05019794 from the NRF of Korea. B.-N.J. is supported by the Basic Science Research Program through the NRF of Korea, funded by the Ministry of Education, Science and Technology (MEST) (2018R1C1B6005768). The International Research & Development Program of the NRF of Korea, funded by the Ministry of Science, ICT & Future Planning (grant no. 2015K1A4A3047851) also funded C.L. The Ewha Womans University Professorship is supported in part by the Ewha Womans University research grant of 2017–2019. This study is also supported in part by operational funds from The First Affiliated Hospital of Xi'an Jiaotong University.

Author contributions

S.-H.L. and H.S.K. collected and analysed the clinical data. S.-H.L., S.-Y.C., Y.Y., C.P. and K.W.Y. wrote the manuscript. J.Y.K., S.W., J.-S.P., G.M.W., C.L. and H.P. revised the manuscript. S.-H.L., S.-Y.C., C.P. and G.K. analysed the 16S rRNA sequences and transcriptomics data. J.-J.J., B.-N.J., H.-S.Y. and Sarang Kim performed the cytometry analysis. Y.Y., J.S., S.L., Y.Y.K., Sujeong Kim, Yunjae Kim and S.G.K. performed the syngeneic mouse model experiments. Seonggon Kim. and J.-S.P. performed the orthotopic mouse model experiments. C.A., E.J.L., Yeongmin Kim and H.K. cultured the bacteria. H.-S.Y. and Sarang Kim performed the in vitro T-cell assays. M.J., H.C. and M.H.N. analysed metabolomics data. G.B.L. and M.H.M. analysed the lipidomics data. K.W.Y. and H.P. designed and supervised all experiments and analyses.

Competing interests

The authors declare no competing interests.

Additional information

Extended data is available for this paper at <https://doi.org/10.1038/s41564-020-00831-6>.

Supplementary information is available for this paper at <https://doi.org/10.1038/s41564-020-00831-6>.

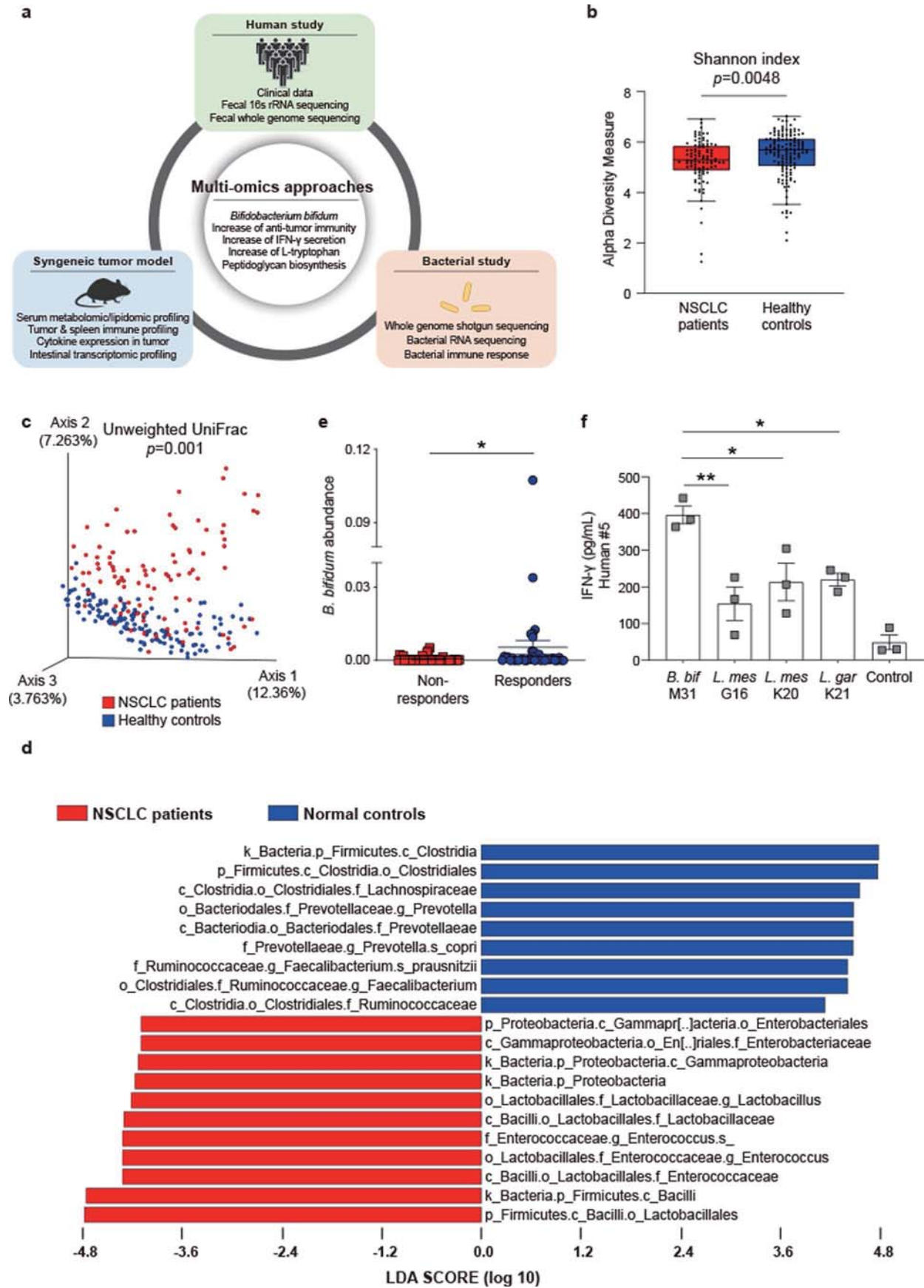
Correspondence and requests for materials should be addressed to K.W.Y. or H.P.

Peer review information *Nature Microbiology* thanks the anonymous reviewers for their contribution to the peer review of this work.

Reprints and permissions information is available at www.nature.com/reprints.

Publisher's note Springer Nature remains neutral with regard to jurisdictional claims in published maps and institutional affiliations.

© The Author(s), under exclusive licence to Springer Nature Limited 2021

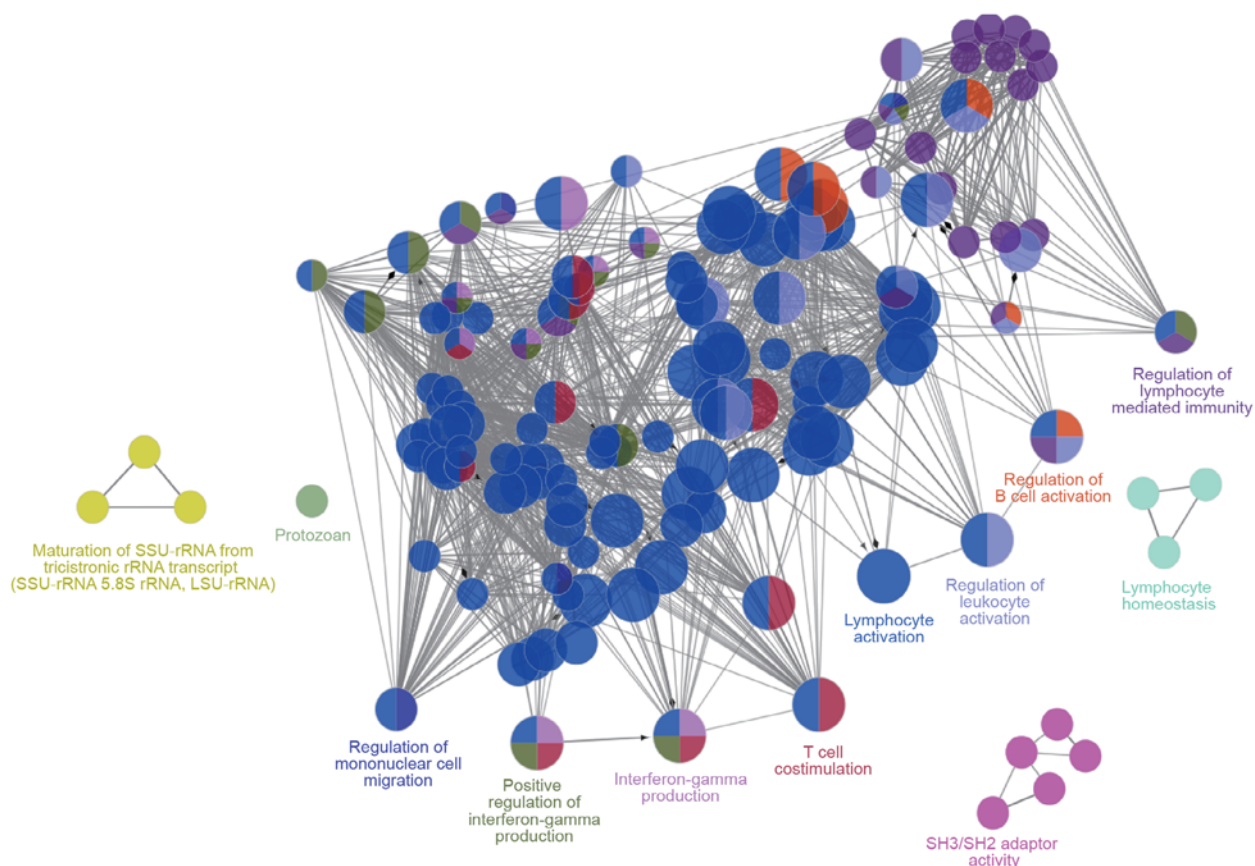


Extended Data Fig. 1 | Comparison of gut microbiome composition between non-small cell lung cancer (NSCLC) patients and healthy controls.

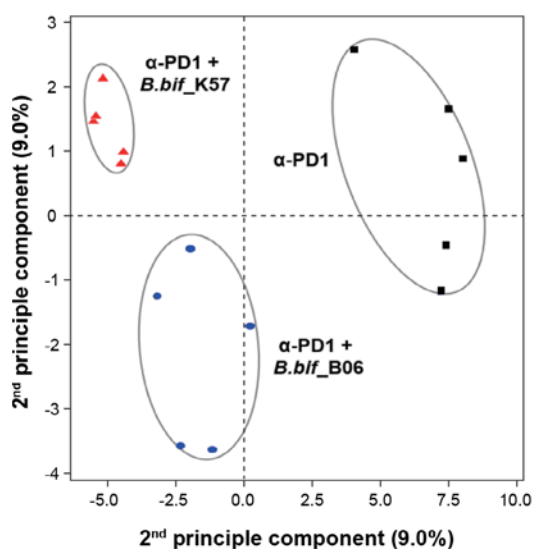
a, Scheme for human, syngeneic tumour model, and bacterial study. **b, c** Box-and-whisker plot illustrating alpha diversity (**b**) and principal coordinate analysis plot illustrating beta diversity (**c**) of gut microbiomes in NSCLC patients (red, $n = 96$) and healthy controls (blue, $n = 139$). p value of alpha diversity calculated using Kruskal-Wallis test. Box represents first, third quartiles, and median, and whiskers are range up to $1.5 \times$ Interquartile Ranges (IQR). **d**, A plot of linear discriminant analysis (LDA) scores from the linear discriminant analysis effect size (LEfSe) method illustrating the differential abundance of the indicated taxa in the gut microbiomes of NSCLC patients (red) and healthy controls (blue) (LDA score > 4). **e**, The abundance of *B. bifidum* in NSCLC patients except epidermal growth factor receptor (EGFR) tyrosine kinase inhibitor (TKI)-treated patients was determined by qPCR ($n = 80$). Data show means \pm SEM. p value calculated using two-sided unpaired Mann-Whitney U test, $p = 0.0128$. **f**, Effect of *B. bifidum* and *Leuconostoc* strains on in vitro stimulation of CD8⁺ T cells by monocytes. Secreted IFN- γ was measured by ELISA in co-cultures of human autologous T cells and monocytes treated with *B. bifidum* and *Leuconostoc* strains (Supplementary Table 5). 3 technical replicates. Data show means \pm SEM. p values calculated using one-way ANOVA with Tukey for multiple comparison. *B. bif_M31* versus *L. mes_G16*, $p = 0.0040$; *B. bif_M31* versus *L. mes_K20*, $p = 0.0245$; *B. bif_M31* versus *L. gar_K21*, $p = 0.0301$. For all graphs, * $p < 0.05$, and ** $p < 0.01$.

Extended Data Fig. 2 | Synergistic anti-tumor effect of *B. bifidum* strains in combination with oxaliplatin or anti-PD-1 in syngeneic mouse tumor models. **a**, Abundance of *B. bifidum* in the mouse intestine after administration. Mice were administered a onetime dose of 1×10^9 CFU of *B. bif_K57* and stool samples were collected at 4, 8, 12, and 24 hr after administration. *B. bifidum* abundance was determined using a qPCR assay with *B. bifidum* specific primers and normalized to 16S rRNA. $n = 5$ independent biological replicates. Data show means \pm SEM. **b**, Flow cytometry analyses were performed on mouse spleen and tumor tissue. Upper: Heatmap represents the p values of differences in immune cell profile between oxaliplatin treatment and combined treatment with oxaliplatin and *B. bifidum* strains. p values calculated using two-sided unpaired t test. The exact p values are provided in Supplementary Table 14. Lower: Ratio of CD8+ T/Treg and effector CD8+ T/Treg in spleen and tumor. Ctrl, $n = 9$; Oxp or Oxp + *B. bif_K57*, $n = 7$; Oxp + *B. bif_B06*, $n = 8$ mice per group. Data show means \pm SEM. p values calculated using one-way ANOVA with Tukey for multiple comparison. Oxp versus Oxp + *B. bif_K57*, $p = 0.0002$ (Ratio of CD8+ T/Treg and effector CD8+ T/Treg, tumor); Oxp versus Oxp + *B. bif_B06*, $p = 0.0124$ (Ratio of effector CD8+ T/Treg, tumor); Oxp versus Oxp + *B. bif_K57*, $p = 0.0011$ (Ratio of CD8+ T/Treg, spleen); Oxp versus Oxp + *B. bif_K57*, $p = 0.0039$ (Ratio of effector CD8+ T/Treg, spleen). **c**, Cytokine expression profiles in tumours from mice treated with oxaliplatin or both oxaliplatin and *B. bifidum* were measured by qPCR. Ctrl or Oxp groups, $n = 6$ independent biological replicates/group; oxaliplatin + *B. bif_K57* or *B. bif_B06* groups, $n = 8$ independent biological replicates/group. Data show means \pm SEM. p values calculated using one-way ANOVA with Tukey for multiple comparison within oxaliplatin treated groups. IFN- γ of Oxp versus Oxp + *B. bif_K57*, $p = 0.0478$; IL-2 of Oxp versus oxp + *B. bif_K57*, $p < 0.0001$; IL-2 of Oxp versus Oxp + *B. bif_B06*, $p = 0.0006$; TNF- α of Oxp versus Oxp + *B. bif_K57*, $p = 0.0004$; TNF- α of Oxp versus Oxp + *B. bif_B06*, $p = 0.0040$; IL-10 of Oxp versus Oxp + *B. bif_K57*, $p < 0.0001$; IL-10 of Oxp versus Oxp + *B. bif_B06*, $p = 0.0063$. **d**, Representative tumor growth curves after administration of *B. bif_M31*, with or without anti-PD-1 treatment. IgG, $n = 8$; anti-PD-1, $n = 5$; *B. bif_M31*, $n = 10$; anti-PD-1 + *B. bif_M31*, $n = 9$ mice per group. Data show means \pm SEM. p value calculated using two-way ANOVA with Tukey for multiple comparison. anti-PD-1 versus anti-PD-1 + *B. bif_M31*, $p < 0.0001$. **e**, Representative tumor growth curves after administration of *B. bif_C01*, with or without anti-PD-1 treatment. IgG, $n = 6$; anti-PD-1 or *B. bif_C01* or and anti-PD-1 + *B. bif_C01*, $n = 7$ mice per group. Data show means \pm SEM. p value calculated using two-way ANOVA with Tukey for multiple comparison. **f**, Flow cytometry analysis of CD4+ T, NK and Treg cells in lamina propria of the intestine. $n = 7$ mice per group. Data show means \pm SEM. p values calculated using one-way ANOVA with Tukey for multiple comparison. CD4+ T cells of anti-PD-1 versus anti-PD-1 + *B. bif_K57*, $p = 0.0015$; NK cells of anti-PD-1 versus anti-PD-1 + *B. bif_K57*, $p = 0.0037$. For all graphs, * $p < 0.05$, ** $p < 0.01$, *** $p < 0.001$, and ns = not significant.

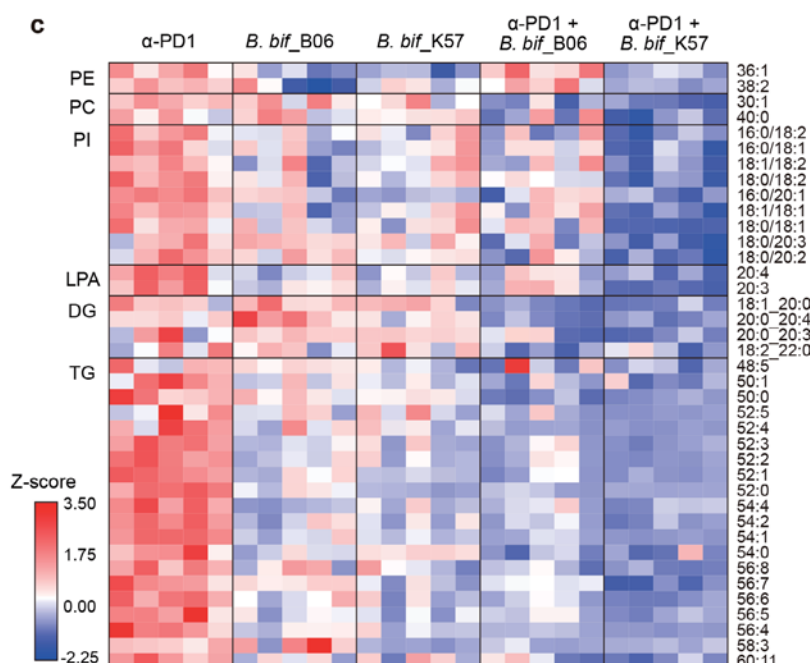
a



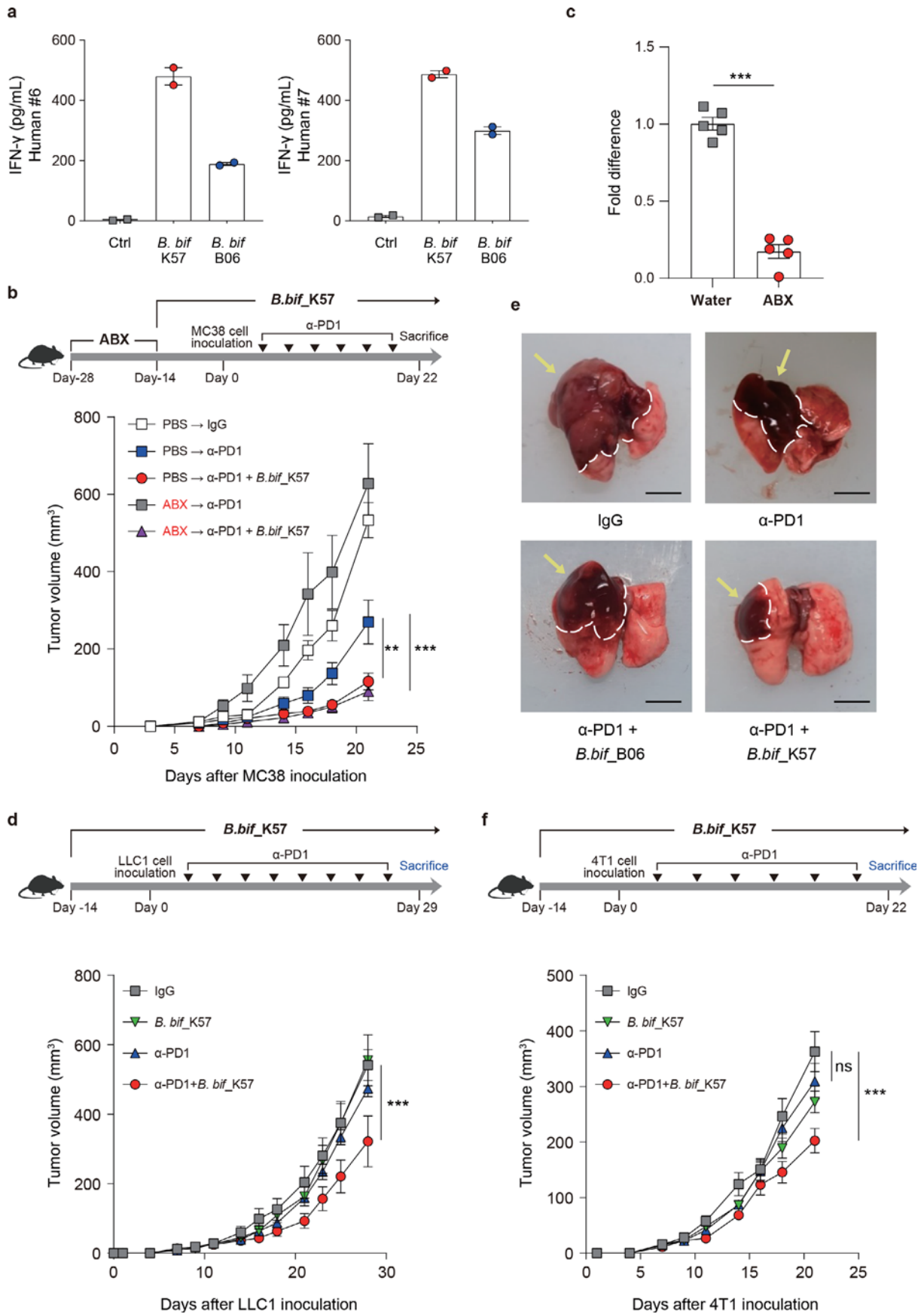
b



c



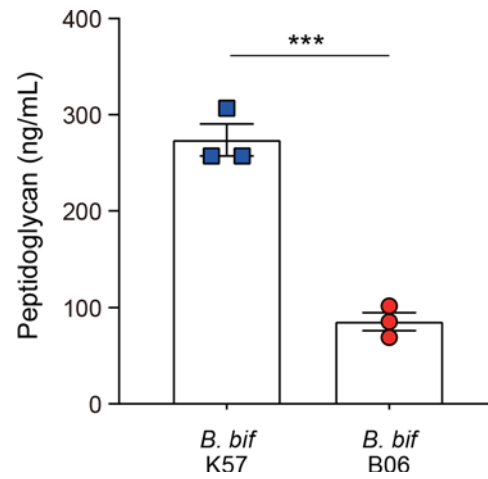
Extended Data Fig. 3 | Transcriptomic and Lipidomic analysis of syngeneic tumor model treated with *B. bifidum* strains. **a, Network representation of enriched Gene Ontology (GO) biological pathways among differentially up-regulated genes in mice treated with anti-PD-1 + *B. bif_K57* mice, determined using ClueGO. **b**, Principal component analysis of syngeneic mouse serum lipid profiles, based on lipids differential abundance among mice treated with anti-PD-1, anti-PD-1 + *B. bif_B06*, and anti-PD-1 + *B. bif_K57* (>1.5-fold & $p < 0.01$). **c**, Heatmap of lipids showing significant differences (>1.5-fold & $p < 0.01$) in serum of syngeneic mice, as revealed by the lipidomic analysis. PE, phosphatidylethanolamine; PI, phosphoinositol; PC, phosphatidylcholine; LPA, lysophosphatidylglycerol; DG, diacylglycerol; TG, triglycerol.**



Extended Data Fig. 4 | See next page for caption.

Extended Data Fig. 4 | Synergistic anti-tumor effect of *B. bifidum* strains in combination with anti-PD-1 in various syngeneic mouse tumor models.

a, Effect of *B. bifidum* strains on in vitro stimulation of CD8 T+ cells by monocytes. Secreted IFN- γ was measured by ELISA in co-cultures of human autologous T cells and monocytes treated with *B. bif_K57* or *B. bif_B06*. 2 technical replicates. Data show means \pm SEM. **b**, Upper: Experimental timeline: Animals were treated with the antibiotic cocktail (ABX) for 14 days. *B. bif_K57* was then orally administered for 14 days before inoculation with MC38 colon cancer cells, followed by administration of anti-PD-1 via intraperitoneal injection twice a week for 21 days. Lower: MC38 tumor growth curves are shown for animals subjected to the indicated experimental treatments. IgG after PBS or anti-PD-1 after PBS, $n = 5$; anti-PD-1 + *B. bif_K57* after PBS, $n = 6$; anti-PD-1 after ABX, $n = 5$; anti-PD-1 + *B. bif_K57* after ABX, $n = 7$ mice per group. Data show means \pm SEM. p values calculated using two-way ANOVA with Tukey for multiple comparison. anti-PD-1 after PBS versus anti-PD-1 + *B. bif_K57* after PBS, $p = 0.0053$; anti-PD-1 after PBS versus anti-PD-1 + *B. bif_K57* after ABX, $p = 0.0004$. **c**, Effect of ABX treatment on the abundance of gut microbiome. Stool 16S rRNA genes were analyzed by qPCR. $n = 5$ mice per group. Data show means \pm SEM. p value calculated using two-sided unpaired t test, $p < 0.0001$. **d**, Upper: Experimental timeline: 14 days after initial oral administration of *B. bif_K57*, mice were inoculated with LLC1. anti-PD-1 was administered via intraperitoneal injection eight times, twice a week for 28 days. Lower: LLC1 tumor growth curves were generated for animals subjected to the indicated experimental treatments. $n = 6$ mice per group. Data show means \pm SEM. p values calculated using two-way ANOVA with Tukey for multiple comparison. IgG versus anti-PD-1 + *B. bif_K57*, $p < 0.0001$. **e**, Macroscopic findings of tumor-inoculated lungs at day 23. The implanted tumors are indicated by yellow arrows. Scale bar, 50 mm. **f**, Upper: Experimental timeline: 14 days after initial oral administration of *B. bif_K57*, mice were inoculated with 4T1 breast cancer cells. anti-PD-1 was administered via intraperitoneal injection six times, twice a week for 21 days. Lower: 4T1 tumor growth curves were generated for animals subjected to the indicated experimental treatments. $n = 10$ mice per group. Data show means \pm SEM. IgG versus anti-PD-1 + *B. bif_K57*, $p < 0.0001$. For all graphs, ** $p < 0.01$, *** $p < 0.001$, and ns = not significant.



Extended Data Fig. 5 | The abundance of peptidoglycan in *B. bifidum* strains. The abundance of peptidoglycan of *B. bif*_K57 and *B. bif*_B06 was estimated using ELISA. Data show means \pm SEM. 3 biological replicates. p value calculated using two-sided unpaired t test, $p < 0.0006$. For all graphs, *** $p < 0.001$.

Reporting Summary

Nature Research wishes to improve the reproducibility of the work that we publish. This form provides structure for consistency and transparency in reporting. For further information on Nature Research policies, see our [Editorial Policies](#) and the [Editorial Policy Checklist](#).

Statistics

For all statistical analyses, confirm that the following items are present in the figure legend, table legend, main text, or Methods section.

n/a Confirmed

- The exact sample size (n) for each experimental group/condition, given as a discrete number and unit of measurement
- A statement on whether measurements were taken from distinct samples or whether the same sample was measured repeatedly
- The statistical test(s) used AND whether they are one- or two-sided
Only common tests should be described solely by name; describe more complex techniques in the Methods section.
- A description of all covariates tested
- A description of any assumptions or corrections, such as tests of normality and adjustment for multiple comparisons
- A full description of the statistical parameters including central tendency (e.g. means) or other basic estimates (e.g. regression coefficient) AND variation (e.g. standard deviation) or associated estimates of uncertainty (e.g. confidence intervals)
- For null hypothesis testing, the test statistic (e.g. F , t , r) with confidence intervals, effect sizes, degrees of freedom and P value noted
Give P values as exact values whenever suitable.
- For Bayesian analysis, information on the choice of priors and Markov chain Monte Carlo settings
- For hierarchical and complex designs, identification of the appropriate level for tests and full reporting of outcomes
- Estimates of effect sizes (e.g. Cohen's d , Pearson's r), indicating how they were calculated

Our web collection on [statistics for biologists](#) contains articles on many of the points above.

Software and code

Policy information about [availability of computer code](#)

Data collection

Flow cytometry data : BDFACS Diva software v8.0.2
 QPCR : CFX384 (Bio-Rad) and StepOnePlus (Applied Biosystems)
 Illumina sequencing : Illumina Miseq platform, Illumina Hiseq platform
 Lipidomic profiling : Lipilot
 Metabolomic profiling : Progenesis QI software (Waters), MassLynx software (Waters)

Data analysis

Metagenomic 16S rRNA sequencing data analysis: Qiime2 v2019.4
 Denoising: DADA2 (qiime2's q2-dada2 plugin)
 taxonomic classification: Qiime2's q2-feature-classifier plugin with the GreenGene database v13_8
 construct reference phylogeny and alignment: Qiime2's q2-fragment-insertion plugin
 Alpha-, beta diversity: Qiime2's q2-diversity plugin
 Differential abundance analysis: LEfSe v1.0
 Raw sequence quality control: FastQC v0.11.5
 Sequencing reads trimming: BBduk from BBmap package v.38.34
 Genome assembler: SPAdes v3.10.1
 Assembly quality assessment: QUAST v4.5
 Bacterial genome annotation: Prokka v1.12
 Construction of the pan genome: Roary v3.11.2
 Identification of SNPs: BactSNP v1.1.0
 Average nucleotide identity (ANI) scores calculation: pyani v0.2.9
 Bacterial RNA sequencing analysis pipeline: READemption v0.4.3
 Mouse RNA sequencing read alignment: STAR v2.5.3a
 RNA-seq gene expression estimation: RSEM v1.3.1
 RNA-seq differential expression analysis: DESeq2 v1.20.0, edgeR v3.21.9

Whole-genome shotgun sequencing: HMP Unified Metabolic Analysis Network (HUMAN2) v.11.2
 Venn diagrams: jvenn v1.9
 Gene Ontology (GO) analysis: ClueGO v2.5.4, Cytoscape v3.3.0
 Flow cytometry: FlowJo v10
 Statistical calculation: Prism 8.4.3 (GraphPad), Rex (Version 3.4.0)
 Difference between two variables: Student's t test
 Difference between multiple variables: ANOVA with Tukey's multiple comparison test
 Associations between two discrete variables: Fisher's exact test

For manuscripts utilizing custom algorithms or software that are central to the research but not yet described in published literature, software must be made available to editors and reviewers. We strongly encourage code deposition in a community repository (e.g. GitHub). See the Nature Research [guidelines for submitting code & software](#) for further information.

Data

Policy information about [availability of data](#)

All manuscripts must include a [data availability statement](#). This statement should provide the following information, where applicable:

- Accession codes, unique identifiers, or web links for publicly available datasets
- A list of figures that have associated raw data
- A description of any restrictions on data availability

16s rRNA and whole genomes sequencing (WGS) data from human stool samples; the mouse intestinal RNA sequencing data; the bacterial WGS data; the bacterial RNA sequencing data have been deposited in the European Nucleotide Archive (accession no. PRJEB26531).

Field-specific reporting

Please select the one below that is the best fit for your research. If you are not sure, read the appropriate sections before making your selection.

Life sciences Behavioural & social sciences Ecological, evolutionary & environmental sciences

For a reference copy of the document with all sections, see [nature.com/documents/nr-reporting-summary-flat.pdf](https://www.nature.com/documents/nr-reporting-summary-flat.pdf)

Life sciences study design

All studies must disclose on these points even when the disclosure is negative.

Sample size	No sample-size calculations were performed. NSCLC patients sample sizes were chosen who diagnosed with incurable stage IIIB and IV NSCLC between January 2016 and August 2017 for continuous follow-up on treatment response, Healthy controls were chosen who underwent a medical check-up between February 2017 and June 2017 to perform 16S ribosomal RNA sequencing concurrently with NSCLC patients. The number of mice assigned to bacteria administration provide sufficient statistic results including tumor size, cytokine and immune profiling. The number of human donors for T cell response experiments was sufficient to show that IFN- γ secretion is determined by the ability of each Bifidobacterium bifidum strains
Data exclusions	We excluded 2 NSCLC patients who treated with systemic targeted therapy just before stool collection, and 15 normal controls who were supplemented with probiotics (n = 11) and antibiotics medication (n = 4).
Replication	Experimental findings were reliably reproduced as described in manuscript and figure legends.
Randomization	Mice were chosen at random for each group prior to administration of B. bifidum strains, and metagenomic results were not need to be randomized in our study.
Blinding	All In vivo studies were not blinded to perform accurately during experiment, and these results were analysed with the appropriate statistical tests to evaluate differences and statistical significance. Flow cytometry and memory T cell assays were performed in a blinded condition.

Reporting for specific materials, systems and methods

We require information from authors about some types of materials, experimental systems and methods used in many studies. Here, indicate whether each material, system or method listed is relevant to your study. If you are not sure if a list item applies to your research, read the appropriate section before selecting a response.

Materials & experimental systems

n/a	Involved in the study
<input type="checkbox"/>	<input checked="" type="checkbox"/> Antibodies
<input type="checkbox"/>	<input checked="" type="checkbox"/> Eukaryotic cell lines
<input checked="" type="checkbox"/>	<input type="checkbox"/> Palaeontology and archaeology
<input type="checkbox"/>	<input checked="" type="checkbox"/> Animals and other organisms
<input type="checkbox"/>	<input checked="" type="checkbox"/> Human research participants
<input checked="" type="checkbox"/>	<input type="checkbox"/> Clinical data
<input checked="" type="checkbox"/>	<input type="checkbox"/> Dual use research of concern

Methods

n/a	Involved in the study
<input checked="" type="checkbox"/>	<input type="checkbox"/> ChIP-seq
<input type="checkbox"/>	<input checked="" type="checkbox"/> Flow cytometry
<input checked="" type="checkbox"/>	<input type="checkbox"/> MRI-based neuroimaging

Antibodies

Antibodies used

For in vivo studies, anti-mouse PD-1 monoclonal antibody (clone RMP1-14, BioXCell, USA, Cat#BE0146), anti-mouse IFN γ R monoclonal antibody (clone GR-20, BioXcell, USA, Cat# BE0029), rat IgG2a isotype control (clone 2A3, BioXCell, BE0089) were used. Anti-human TLR2-IgA antibody (Invivogen, USA, Cat# maba2-hltr2) was used for Fig. 4f

For flow cytometry, anti-mouse-CD45 (Biolegend, Cat# 103116), CD3 (Biolegend, Cat# 100218), NK1.1 (Biolegend, Cat# 108708), CD49b (Biolegend, Cat# 108910), CD4 (Biolegend, Cat#100422), CD25 (Biolegend, Cat#101904), Foxp3 (Invitrogen, Cat#17-5773-82), CD44 (Biolegend, Cat# 103008), CD62L (Biolegend, Cat#104412), CD8a (Biolegend, Cat#100706, spleen and tumor), CD8a (Biolegend, Cat#100712, intestine cytokine expression), IFN- γ (Biolegend, Cat# 505806), and IL-2 (Biolegend, Cat#503820) were used

Validation

All antibodies used in this study were validated by the manufacturers and previous publications as follows

Antibodies for In vivo studies

anti-mouse PD-1 monoclonal antibody (clone RMP1-14, BioXCell, USA, Cat#BE0146), manufacturer's website (<https://bxcell.com/product/invivomab-anti-m-pd-1/>).

anti-mouse IFN γ R monoclonal antibody (clone GR-20, BioXcell, USA, Cat# BE0029), manufacturer's website (<https://bxcell.com/product/m-cd119-ifngammar/>).

rat IgG2a isotype control (clone 2A3, BioXCell, BE0089), manufacturer's website (<https://bxcell.com/product/rat-igg2a-isotype-control/>)

Antibody for in vitro study

anti-human TLR2-IgA antibody (Invivogen, USA, Cat# maba2-hltr2), manufacturer's website (<https://www.invivogen.com/anti-hltr2-iga>).

Antibodies for flow cytometry analysis

anti-mouse CD45 (Biolegend, Cat# 103116), manufacturer's website (<https://www.biolegend.com/en-us/products/apc-cyanine7-anti-mouse-cd45-antibody-2530>).

anti-mouse CD3 (Biolegend, Cat# 100218), manufacturer's website (<https://www.biolegend.com/en-us/products/percp-cyanine5-5-anti-mouse-cd3-antibody-5596>)

anti-mouse NK1.1 (Biolegend, Cat# 108708), manufacturer's website (<https://www.biolegend.com/en-us/products/pe-anti-mouse-nk-1-1-antibody-431>)

anti-mouse CD49b (Biolegend, Cat# 108910), manufacturer's website (<https://www.biolegend.com/en-us/products/apc-anti-mouse-cd49b-pan-nk-cells-antibody-231>)

anti-mouse CD4 (Biolegend, Cat#100422), manufacturer's website (<https://www.biolegend.com/en-us/products/pe-cyanine7-anti-mouse-cd4-antibody-1919>)

anti-mouse CD25 (Biolegend, #101904), manufacturer's website (<https://www.biolegend.com/en-us/products/pe-anti-mouse-cd25-antibody-129>)

anti-mouse Foxp3 (Invitrogen, Cat#17-5773-82), manufacturer's website (<https://www.thermofisher.com/antibody/product/FOXP3-Antibody-clone-FJK-16s-Monoclonal/17-5773-82>)

anti-mouse CD44 (Biolegend, Cat# 103008), manufacturer's website (<https://www.biolegend.com/en-us/products/pe-anti-mouse-human-cd44-antibody-2206>)

anti-mouse CD62L (Biolegend, Cat#104412), manufacturer's website (<https://www.biolegend.com/en-us/products/apc-anti-mouse-cd62l-antibody-381>)

anti-mouse CD44 (Biolegend, Cat# 103008), manufacturer's website (<https://www.biolegend.com/en-us/products/pe-anti-mouse-human-cd44-antibody-2206>)

anti-mouse CD8a (Biolegend, #100712, spleen and tumor), manufacturer's website (<https://www.biolegend.com/en-us/products/fitc-anti-mouse-cd8a-antibody-153>)

anti-mouse CD8a (Biolegend, #100712, intestine cytokine expression), manufacturer's website (<https://www.biolegend.com/en-us/products/apc-anti-mouse-cd8a-antibody-150>)

anti-mouse IFN- γ (Biolegend, Cat# 505806), manufacturer's website (<https://www.biolegend.com/en-us/products/fitc-anti-mouse-ifn-gamma-antibody-995>)

anti-mouse IL-2 (Biolegend, Cat#503820), manufacturer's website (<https://www.biolegend.com/en-us/products/pacific-blue-anti-mouse-il-2-antibody-4138>)

Eukaryotic cell lines

Policy information about cell lines

Cell line source(s)

MC38 cell line was purchased from Kerafast (Cat# EZH204). LLC1 cell line was purchased from ATCC (Cat# CRL1642) and 4T1

Cell line source(s)	cell line was purchased from ATCC (Cat# CRL-2539) For orthotopic lung cancer model, Lewis lung cancer cells (LLC) expressing an enhanced firefly luciferase (effluc) gene were donated by Dr. Yong Hyun Jeon (DGMIF, Korea).
Authentication	MC38, LLC1, and 4T1 cell lines were authenticated using DNA fingerprint analysis.
Mycoplasma contamination	MC38, LLC1, and 4T1 cell lines were negative for mycoplasma contamination
Commonly misidentified lines (See ICLAC register)	No commonly misidentified cell lines were used in the study.

Animals and other organisms

Policy information about [studies involving animals](#); [ARRIVE guidelines](#) recommended for reporting animal research

Laboratory animals	C57B6/N mice (female) were provided by Orient Bio (Gapyeong, Gyeonggi, Korea) for MC38 and LLC1 tumor mice. C57B6/N mice (male) were provided by Orient Bio for orthotopic tumor model for LLC1 tumor mice. BALB/c mice (female) were provided by Orient Bio for 4T1 tumor mice. TLR2 KO mice (female) were purchased from the Jackson Laboratories. The mice were maintained on the 12hr/12hr light/dark cycle (light period 7:00 am - 7:00 pm) at ambient temperature (20°C - 24°C) and 45-55% humidity.
Wild animals	No wild animals were used in the study.
Field-collected samples	No field-collected samples were used in the study
Ethics oversight	All animal experiments were carried out in accordance with protocols approved by the Institutional Animal Care and Use Committee of CHA University, Gwangju Institute of Science and Technology Animal Care and Use Committee, and Daegu-Gyeongbuk Medical Innovation Foundation (DGMIF). All animals used in this study were maintained and handled according to the policies approved study protocols.

Note that full information on the approval of the study protocol must also be provided in the manuscript.

Human research participants

Policy information about [studies involving human research participants](#)

Population characteristics	The detailed information is provided in the Supplementary Tables 1-3. We described clinical data about the participants, including BMI, smoking history, alcohol history, stool collection time and serum glucose level, and the clinical characteristics, including age, sex, smoking status, alcohol status, histologic type, glucose, and BMI, were not significantly different between responders and non-responders
Recruitment	Healthy controls (n = 154) underwent a medical check-up at Seoul National University Hospital (SNUH) between February 2017 and June 2017; none had a serious illness at the time of examination. Healthy controls who underwent antibiotic (n = 4) or probiotic (n = 11) treatment within 3 months before the stool collection were excluded from the study. NSCLC patients enrolled in this study were diagnosed with stage IIIB or IV NSCLC through the standardized review performed by expert pathologists at Samsung Medical Center (SMC) between January 2016 and August 2017 (n = 98). Patients were excluded from the study if they received antibiotic or probiotic treatment within 3 months before the stool collection.
Ethics oversight	Stool samples were obtained with informed consent at the SMC and SNUH, and the study was approved by the institutional review board in accordance with the Declaration of Helsinki (2008-06-033 and 1609-051-790, respectively).

Note that full information on the approval of the study protocol must also be provided in the manuscript.

Flow Cytometry

Plots

Confirm that:

- The axis labels state the marker and fluorochrome used (e.g. CD4-FITC).
- The axis scales are clearly visible. Include numbers along axes only for bottom left plot of group (a 'group' is an analysis of identical markers).
- All plots are contour plots with outliers or pseudocolor plots.
- A numerical value for number of cells or percentage (with statistics) is provided.

Methodology

Sample preparation

The detailed information is provided in the methods section. Dissected tumors were cut into small pieces and transferred in RPMI 1640 media (GIBCO Invitrogen) supplemented with collagenase type 1 at 2.5 mg/mL, collagenase type 2 at 1.5 mg/mL, collagenase type 4 at 1 mg/mL, DNase Type1 at 50 µg/mL and hyaluronidase Type IV-S at 0.25 mg/mL for 50 min at 37°C and filtered using 70 µm cell strainer (BD Bioscience, San Jose, USA). Spleens were mashed in RPMI 1640 media and RBC lysed using RBC lysis buffer (eBioscience, San Diego, USA) and filtered using 70 µm cell strainer. Lamina propria cells were isolated from the large intestine according to isolation protocols (Ferrer-Font et al. 2020)

	Splenocytes, tumor cells, and lamina propria cells were incubated with anti-mouse CD16/CD32 (BD Bioscience) at 10 min at 4°C for Fc receptor block.
Instrument	Canto II flow cytometer (BD Bioscience, San Jose, USA).
Software	DIVA (BD Bioscience) was used for data collection and FlowJo software (LLC) was used for flow cytometric data analysis
Cell population abundance	The study doesn't include any experiments with sorted cells
Gating strategy	<p>The detailed information is provided in the Supplementary Information Fig. 1 and 2</p> <p>Gate 1 : FSC-A/SSC-A parameters were used for cells gating</p> <p>Gate 2 : FSC-H/FSC-A parameters were used to excluded doublets</p> <p>Gate 3 : SSC-A/APC-Cy7-A;CD45 parameters were used for immune cells gating</p> <p>Gate 4 : PerCP-Cy5.5-A;CD3 parameters were used for dividing NK cells and T cells identification</p> <p>Gate 5 : APC-A;CD49b/PE-A;NK1.1 cells parameters were used for NK cells identifying</p> <p>Gate 6 : FITC-A;CD8/PE-Cy7-A;CD4 parameters were used for CD4+ and CD8+ T cells identification</p> <p>Gate 7 : APC-A;CD62L/PE-A;CD44 parameters were used for effector cell identification</p> <p>Gate 8 : PE-A;CD25/APC-A;Foxp3 parameters were used for Treg cells identification</p> <p>Gate : APC-A;CD8/FITC-A;IFN-γ parameters were used for CD8+IFNγ+ identification</p> <p>Gate : PE-Cy7-A;CD4/Pacific Blue-A;IL-2 parameters were used for CD4+IL-2+identification</p>

Tick this box to confirm that a figure exemplifying the gating strategy is provided in the Supplementary Information.